12-2022

Developing a Methane Detector for Aerospace Applications

Michael A. Kirk
Utah State University

DEVELOPING A METHANE DETECTOR FOR AEROSPACE APPLICATIONS

by

Michael A. Kirk

A thesis submitted in partial fulfillment
of the requirements for the degree

of

MASTER OF SCIENCE

in

Mechanical Engineering

Approved:

Nick Roberts, Ph.D. Major Professor	Charles Swenson, Ph.D. Committee Member
David Geller, Ph.D. Committee Member	D. Richard Cutler, Ph.D. Vice Provost for Graduate Studies

UTAH STATE UNIVERSITY
Logan, Utah

2022

ABSTRACT

Developing a Methane Detector for Aerospace Applications

by

Michael A. Kirk, Master of Science

Utah State University, 2022

Major Professor: Nick Roberts, Ph.D.
Department: Mechanical and Aerospace Engineering

CH_4 is one of the most impactful greenhouse gasses, second only to CO_2. The purpose of this project is to further a new technology for detecting CH_4 leaks called FINIS (Filter Incidence Narrow-band Infrared Spectrometer), thus improving our capability to detect CH_4 leaks and reduce greenhouse gas emissions. FINIS has been developed in various stages since 2018 and has been accepted to fly on the ACMES (Active Cooling for Multispectral Earth Sensors) mission in 2024. My thesis will explore a new and optimized design for FINIS to be implemented on a CubeSat and determine whether it can survive the space environment. As part of the design and testing process, we will determine whether the precision of the FINIS instrument is comparable to other CH_4 missions. FINIS is estimated to be more compact, capable, and affordable than previous remote-sensing aerial and space sensors and has the potential for providing a next-generation CH_4 sensor.

(92 pages)

PUBLIC ABSTRACT

Developing a Methane Detector for Aerospace Applications

Michael A. Kirk

Greenhouse gasses in the atmosphere are raising the global temperature and causing adverse side effects. Of these greenhouse gasses, methane is one of the most impactful, second only to carbon dioxide. One of the methods for determining the concentration of methane in the atmosphere is taking images of the earth from space. The purpose of this project is to further a new imaging technology for detecting methane leaks called FINIS (Filter Incidence Narrow-band Infrared Spectrometer), thus improving our capability to detect and locate methane leaks and reduce greenhouse gas emissions. FINIS has been developed in various stages since 2018 and has been accepted to fly on a CubeSat called ACMES (Active Cooling for Multispectral Earth Sensors) in 2024. My thesis will explore a new and optimized design for FINIS to be implemented on a CubeSat and determine whether it can survive the space environment. As part of the design and testing process, we will determine whether the precision of the FINIS instrument is comparable to other satellites observing methane. FINIS is estimated to be more compact, capable, and affordable than previous space-based sensors and has the potential for providing a next-generation methane sensor.

CONTENTS

Page

LIST OF TABLES

LIST OF FIGURES

ACRONYMS

ACMES	Active Cooling for Multispectral Earth Sensors
ADC	Analog to Digital Converter
AOI	Angle of Incidence
ASI	Agenzia Spaziale Italiana
ATA	Active Thermal Architecture
CH_4	Methane
CO	Carbon Monoxide
CO_2	Carbon Dioxide
COTS	Commercial Off The Shelf
CSE	Center for Space Engineering
CWL	Center Wavelength
DIAL	Differential Absorption Lidar
DOAS	Differential Optical Absorption Spectroscopy
ESA	European Space Agency
FINIS	Filter Incidence Narrow-band Infrared Spectrometer
FOV	Field of View
FPA	Focal Plane Array
FWHM	Full Width Half Maximum
GHG	GreenHouse Gas
GHGSat	GreenHouse Gas Satellite
GOSAT	Greenhouse gases Observing Satellite
HITRAN	HIgh-resolution TRANsmission molecular absorption database
HyTI	Hyperspectral Thermal Imager
InGaAs	Indium Gallium Arsenide
JAXA	Japan Aerospace Exploration Agency
LWIR	Long-wave Infrared
MWIR	Mid-wave Infrared

NSO	Netherlands Space Office
OOB	Out of Band
PLAID	Planar Langmir Impedance Detector
ppb	parts per billion
PRISMA	PRecursore IperSpettrale della Missione Applicativa
PSF	Point Spread Function
SCIAMACHY	SCanning Imaging Absorption spectroMeter for Atmospheric CHartographY
SNR	Signal to Noise Ratio
SWIR	Short-wave Infrared
SZA	Solar Zenith Angle
TANSO	Thermal And Near infrared Sensor for carbon Observation
TANSO-CAI-2	TANSO - Cloud and Aerosol Imager-2
TANSO-FTS-2	TANSO - Fourier Transform Spectrometer-2
TEC	ThermoElectric Cooler
TDLAS	Tuneable Diode-Laser Absorption Spectroscopy
TROPOMI	Tropospheric Monitoring Instrument
USU	Utah State University

CHAPTER 1

INTRODUCTION

1.1 The ACMES Mission

ACMES is a technology demonstration mission featuring an active thermal architecture (ATA) and three scientific payloads. The 12U CubeSat is expected to launch on a SpaceX Falcon 9 in 2024. The primary technology that will be demonstrated on the mission, ATA, is an active thermal control of cryogenic instruments on small satellites. ATA will be cooling an instrument from the University of Hawaii called HyTI (Hyperspectral Thermal Imager). HyTI is a high spectral and spatial long-wave infrared imager with a focus on volcanic degassing, land surface temperature, and precision agriculture metrics [1]. The two other payloads, PLAID and FINIS, are student projects from Utah State University (USU). PLAID (Planar Langmir Impedance Detector) will observe pre-conditions of the ionosphere leading to plasma bubbles. The FINIS instrument is the focus of this thesis and is being developed with the goal of becoming a next-generation CH_4 (methane) sensor.

1.2 Why Methane?

The atmosphere is composed of various concentrations of gases that separate the earth's surface from space. While the atmosphere is necessary for human survival by protecting us from radiation and elevating the surface to a sustainable temperature, anthropogenic sources are increasing the concentration of greenhouse gases in the atmosphere and leading to global warming. CH_4 is the second most abundant greenhouse gas, accounting for about 20 percent of global greenhouse gas emissions. While atmospheric CH_4 is only about 0.5% as abundant as CO_2 (carbon dioxide), CH_4 is more than 25 times as effective as CO_2 at trapping heat in the atmosphere [2]. CH_4 also has a much shorter lifetime in the atmosphere (12 years compared to centuries for CO_2), meaning reductions in CH_4 emissions will have

a much more immediate impact on global warming.

CH_4 emissions are easier to monitor and control than CO_2 emissions, making reducing CH_4 the most cost-effective strategy for reducing global greenhouse emissions. Most CH_4 emissions are human caused, with the majority of human caused CH_4 emissions coming from three sectors: fossil fuels (35 percent of human caused emissions), waste (20 percent), and agriculture (40 percent) [3]. Over the past decade, these sources have caused the background atmospheric CH_4 concentration to increase by about 5% (see Fig. 1.1). FINIS will aid in locating CH_4 leaks so efforts can be made to reduce the amount entering the atmosphere.

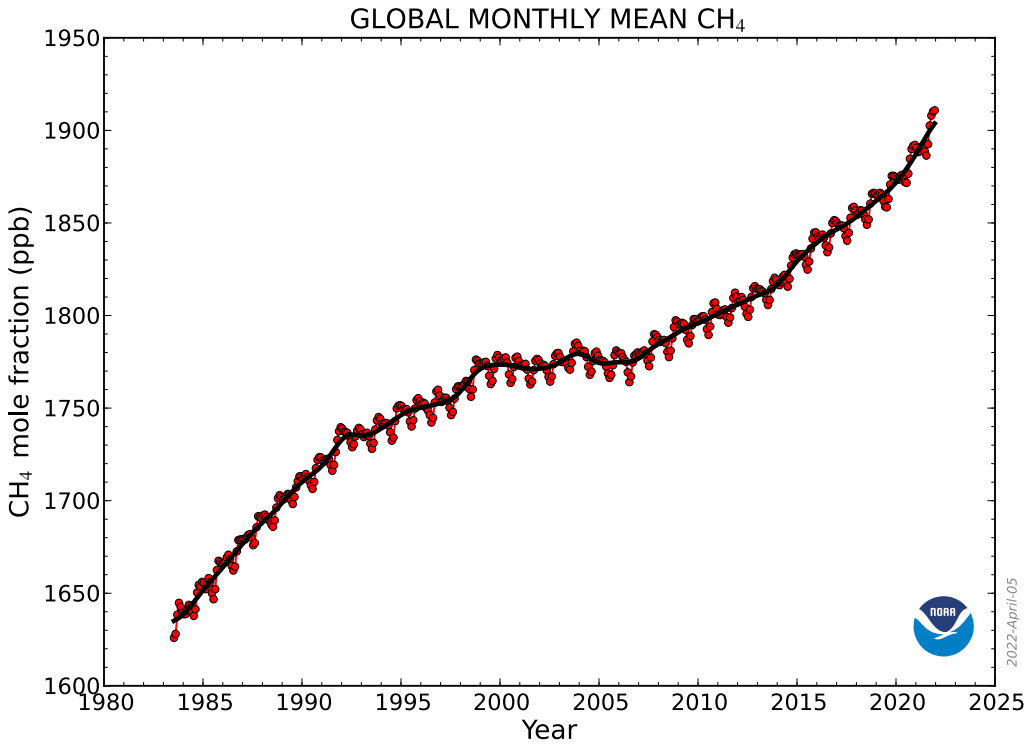

Fig. 1.1: CH_4 Trend [4]

1.3 Methods for detecting CH_4

The goal to reduce CH_4 starts with detecting point source leaks. Methods for detecting CH_4 can generally be categorized as either in-situ or remote. In-situ methods require capturing samples of the CH_4 plume and analyzing the ingested gas by optical or chemical means. Monitoring a large number of facilities or pipelines with in-situ methods is impractical due to the number of sensors that would be needed to measure potential leaks on a large scale. Remote sensors, on the other hand, are ideal for global CH_4 mapping because satellites and other remote sensing methods can cover a much larger area.

Like FINIS, most remote sensing solutions are optical sensors in active (laser-based) or passive camera configurations. Laser-based systems using tunable diode-laser absorption spectroscopy (TDLAS) or differential absorption lidar (DIAL) sensors have very good sensitivity for point observation, but are insufficient for covering wide areas. Passive systems include thermal sensors or hyperspectral cameras tuned to the strongest CH_4 absorption bands. Because they usually operate in mid-wave infrared (MWIR) and long-wave infrared (LWIR) regions they require a cryocooler for operation, thus limiting their applications due to power and size constraints [5]. FINIS is a passive sensor that operates in the short-wave infrared (SWIR) region, allowing it to operate at room temperature and eliminating the need for a cryocooler.

The temperature a camera sensor needs to be cooled to is dependant on the wavelength being observed. Every object emits radiation based on its temperature, and the camera sensor needs to be cooled to a point that it doesn't emit light in the spectra being observed. Planck's law is used to determine what wavelengths an object emits at a given temperature, and can be used to determine an optimal temperature for camera sensor. An example of this is shown in Figure 1.2. As the temperature of an object decreases, the radiant energy shifts to longer wavelengths.

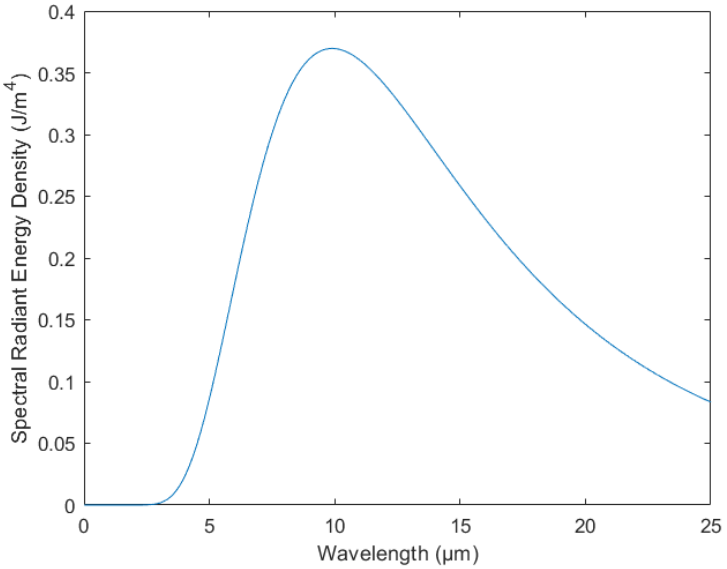

Fig. 1.2: This plot shows the relationship between intensity and wavelength for an object at room temperature (293 K).

CH_4 can be observed at four absorption features as shown in Fig. 1.3. The first absorption band (1.666μm) can be observed using an InGaAs camera. InGaAs cameras generally operate between 0-20° C (273-293 K), removing the need for large and power consuming cryocoolers. TEC's (thermoelectric coolers) are used for temperature stabilization, helping to reduce dark current. The next absorption band at 2.372μm is more sensitive to CH_4 than the 1.666μm band, but the MCT cameras used in this range must be cooled to -73° C (200 K). The 3.311μm and 7.645μm bands need to be cooled to progressively lower temperatures.

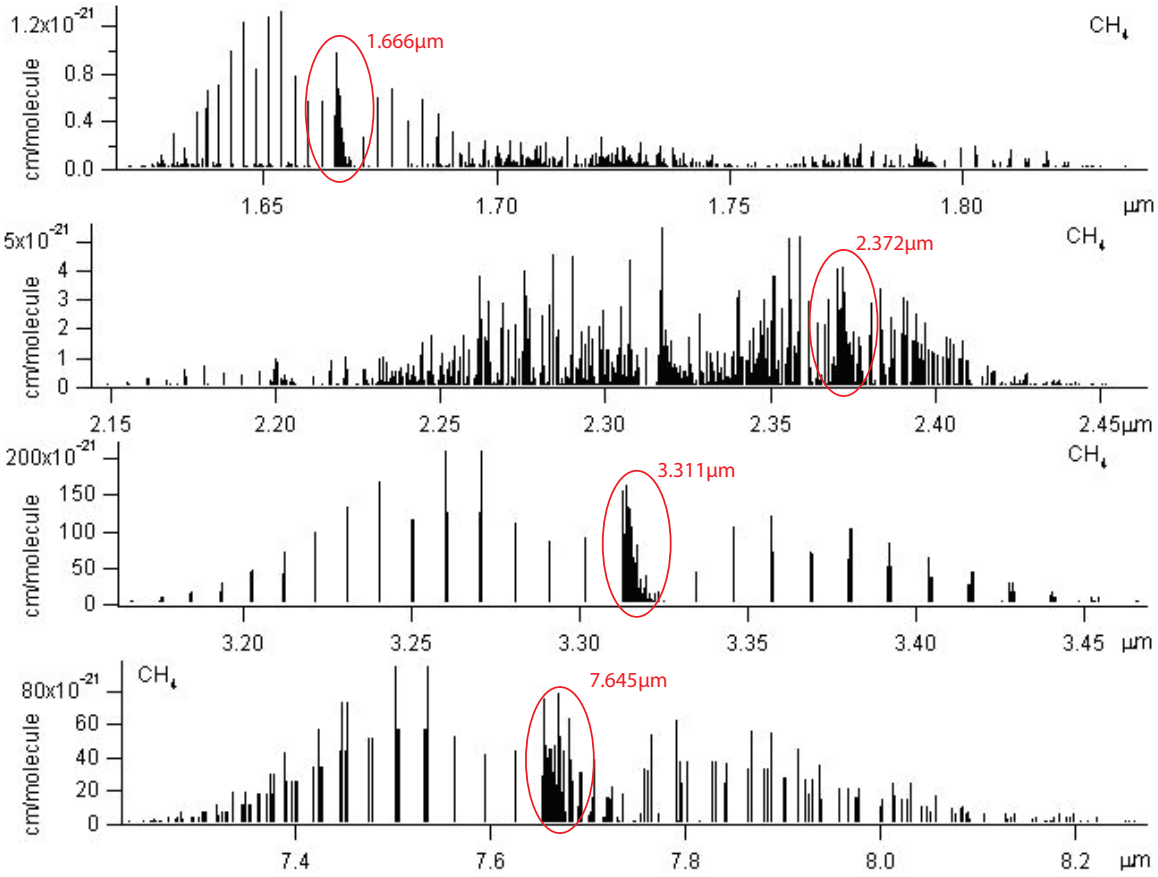

Fig. 1.3: CH_4 absorption bands from Hitran 2004 data [6]

Perhaps more important than the level of cooling needed at each of the absorption bands is the presence of other gases in the spectra. When multiple gases are absorbed at the same wavelength, it becomes difficult to differentiate the contributions from each species. While the 2.3µm, 3.3µm, and 7.6µm bands have stronger absorption features, they are saturated with H_2O and CO_2. FINIS takes advantage of the 1.666µm range for CH_4 measurements as it requires less cooling and is less saturated.

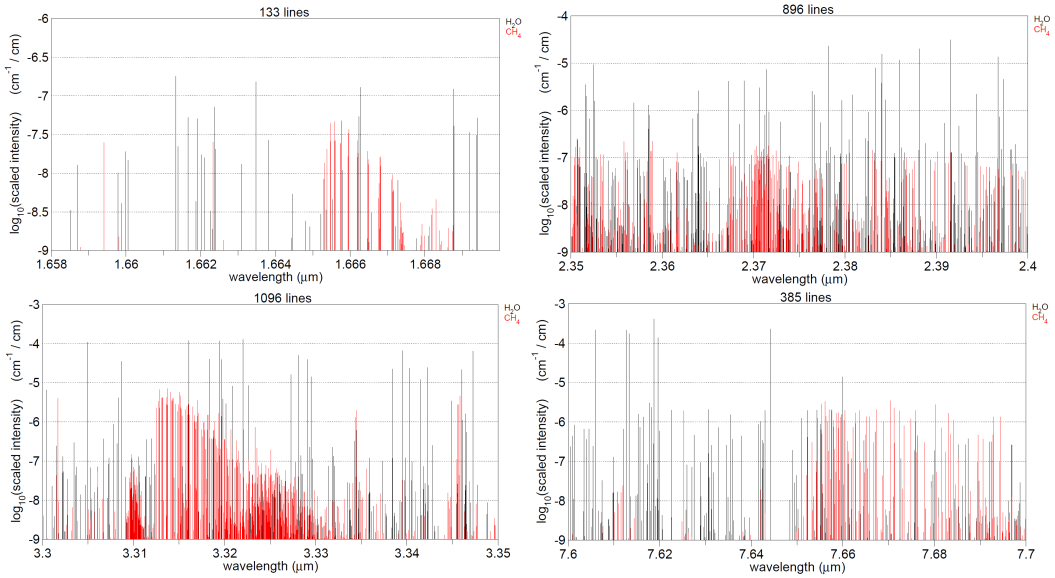

Fig. 1.4: The four CH_4 absorption bands are shown with H_2O lines. H_2O saturates most of the bands, but the 1.66µm band isn't overly saturated. [6]

1.4 CH_4 Observations from Space

Over the past two decades there have been several satellite missions with the goal of measuring atmospheric CH_4 concentrations and detecting point source leaks. Some of the major missions are SCIAMACHY, TROPOMI, GOSAT, PRISMA and GHGSat. Each of these missions use spectrometer technologies to analyze the wavelengths of light entering the sensor. The sensor receives light that travels through the down-welling and up-welling paths as shown in Fig. 1.5. If CH_4 is present in the optical path it will absorb the light at the various absorption bands, leaving a black image at those wavelengths. The concentration of the CH_4 is determined by using a calibrated sensor and comparing pixels in the absorption band and the transmission band. (See Fig. 1.7).

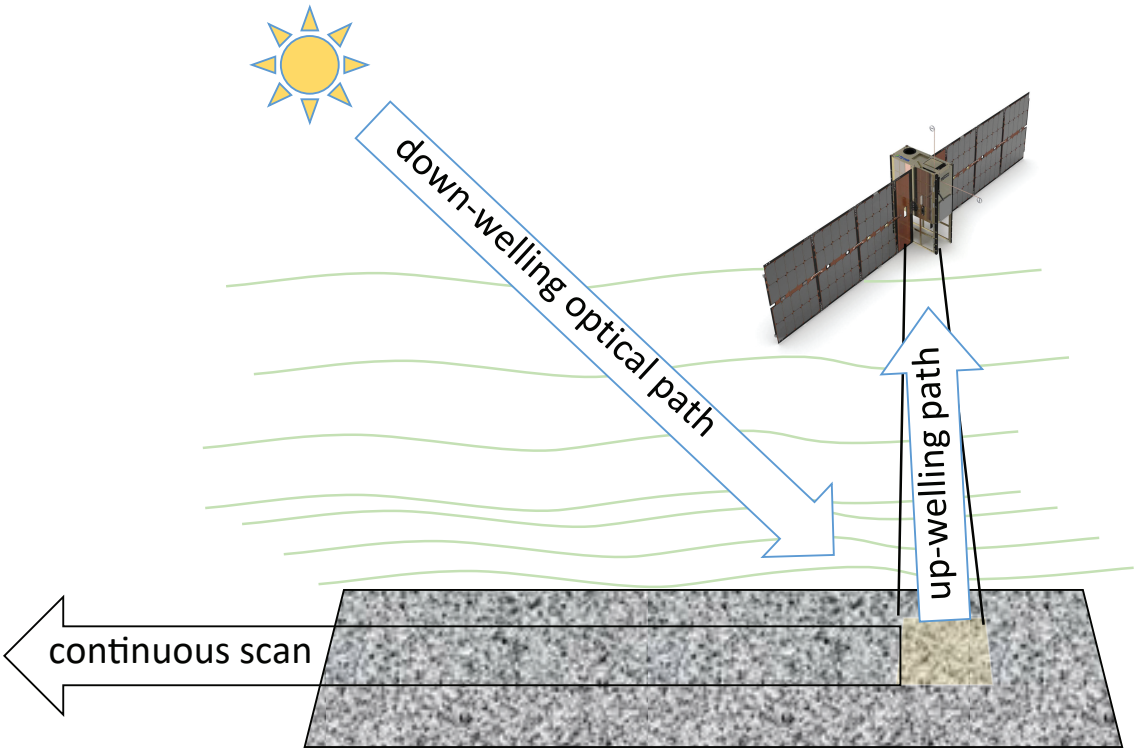

Fig. 1.5: Remote space sensor concept of operations

Some of the parameters for comparing CH_4 satellite missions are measurement sensitivity, spatial resolution, swath, size, mass, and power. The measurement sensitivity is often reported in parts per billion (ppb). As previously shown in Fig. 1.1, the atmospheric background concentration of CH_4 is around 1900 ppb. For an instrument to accurately detect a leak, the leak must be large enough to raise the background CH_4 concentration by the value of the instrument sensitivity. The spatial resolution generally refers to the pixel ground sampling distance, or the smallest object that can be resolved by the sensor. A large spatial resolution limits the instrument to being an area flux mapper that measures CH_4 concentration over a city or state rather than a point source imager that can identify specific leak sites. The swath is the width of each scan when all pixels are considered. Size, mass, and power are crucial for cost effective, repeatable, and scaleable missions.

Individual characteristics of major CH_4 missions are discussed in the following sections.

1.4.1 SCIAMACHY (ESA)

SCIAMACHY was one of the first CH_4 detectors in space, operating from 2002-2012 as a part of the Envisat mission. It used a grating spectrometry technology to observe eight bands including wavelengths for CH_4, CO (carbon monoxide), and CO2. It observed CH_4 using the 2.3 µm spectral lines. The primary scientific objective was the global measurement of various trace gases in the troposphere and stratosphere [7]. SCIAMACHY used a mechanical scan mirror to switch from nadir and limb line of sights for various measurements. The spatial resolution of the instrument was 30 km and it had a swath of 960 km, putting it in the category of an area flux mapper. It was able to measure CH_4 with a sensitivity of 30 ppb. The instrument was 0.7 m^3 in volume, weighed 198 kg, and used 122 W of power [8].

1.4.2 TROPOMI (ESA, NSO)

TROPOMI was one of the first major CH_4 satellites after SCIAMACHY. It was launched in 2017 in collaboration between the European Space Agency (ESA) and the Netherlands Space Office (NSO). TROPOMI also uses grating spectrometry using four spectrometers, each split electronically to cover 8 bands in UV, VIS, NIR, and SWIR spectrums. The instrument is able to measure CH_4 with a sensitivity of 12 ppb. It has a spatial resolution of 7 km and a swath of 2600 km, also putting it in the range of an area flux mapper. TROPOMI weighs 220 kg, uses 170 W, and is 0.68 m^3 [9].

1.4.3 GOSAT-2 (JAXA)

GOSAT-2 was launched in October of 2018 as a follow-up to the original GOSAT mission (launched 2009). The instrument boasts a high signal to noise ratio (SNR), accurate onboard calibration, five spectral bands, and an intelligent pointing system that increases useful data collections in the presence of clouds. The onboard processing detects the least cloudy areas in the field of view (FOV) and shifts the instrument towards unobstructed views before collecting data. The instrument is able to measure CH_4 with a precision of 5 ppb. It has a swath of 1000 km and a spatial resolution of 10 km. Like SCIAMACHY and TROPOMI it is an area flux mapper. It weighs 137 kg, uses 350 W, and is 0.8 m^3 [10].

1.4.4 PRISMA (ASI)

PRISMA is a medium-resolution hyperspectral imaging mission made by the Italian Space Agency and launched in 2019. It uses a pushbroom scanning technique and is able to observe approximately 250 spectral bands. It has a spatial resolution of 30 m and a swath of 30 km, allowing it to act as a point source imager, however it has a low sensitiviy of 60 ppb. The instrument uses a prism spectrometer concept and a passive radiator for cooling down to 185 K. The science instrument weighs 90 kg, uses 110 W, and is 0.35 m^3 [11].

1.4.5 GHGSat (GHGSat, Inc.)

GHGSat is a commercial company based in Canada with the goal of becoming the global reference for the remote sensing of greenhouse gas emissions from any source in the world. Their constellation currently consists of three satellites, GHGSat-D (Claire) launched in 2016, GHGSat-C1 (Iris) launched in September 2020, and GHGSat-C2 (Hugo) launched in January 2021. The satellites use a wide-angle Fabry-Perot spectrometer for measuring column density of greenhouse gases. The -D satellite measures both CH_4 and CO_2, while the -C1 and -C2 satellites are optimized for CH_4. GHGSat has a goal of having a constellation of 10 satellites by 2023. Their latest satellites have a spatial resolution of 25 m, a swath of 12 km, and a sensitivity of 12 ppb making them effective as point source imagers. As the satellite scans the ground it creates a hypercube of stacked images overlapping to increase precision. The instrument weighs 9 kg, uses 45 W, and is 0.004 m^3 [12].

1.5 The Advent of FINIS

USU's Center for Space Engineering (CSE) has been developing FINIS for several years with a team of students and professionals. Prior to being accepted to fly on the ACMES mission it had two rounds of funding, one in 2018 and one in 2019. The first round of funding involved the development of the basic FINIS model and procurement of parts, then the second round involved advancing the design and running an aerial test on a Cessna aircraft. The instrument is shown in Fig. 1.6

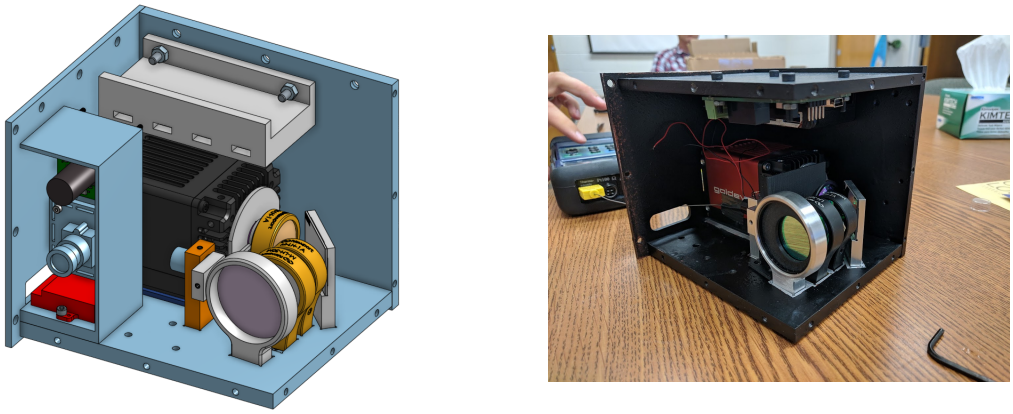

Fig. 1.6: Old FINIS instrument with sides removed

FINIS takes advantage of a CH_4 1666 nm absorption feature to detect CH_4. This falls in the SWIR range allowing FINIS to operate at room temperature and removing the requirement of a cryocooler. At the front of the FINIS optics is a narrow-band filter at a four degree tilt which creates high-resolution hyperspectral images over a narrow spectral band. The line center shifts to shorter wavelengths at non-normal incidence with the filter creating a spectrum of wavelengths with 1666 nm being displayed on one side of the sensor and 1660 nm on the other. As the FINIS instrument scans the ground, images are compared pixel to pixel to create a ratio of the absorption band and the transmission band. This ratio is proportional to the CH_4 column. An example of this process is shown in Fig. 1.7. The image on the left shows a CH_4 balloon in the absorption band, while the same balloon is shown in the right image in the transmission band. The absorption feature causes the balloon to appear black. A ratio of the balloon pixels is used to determine the concentration of CH_4 in the image [5].

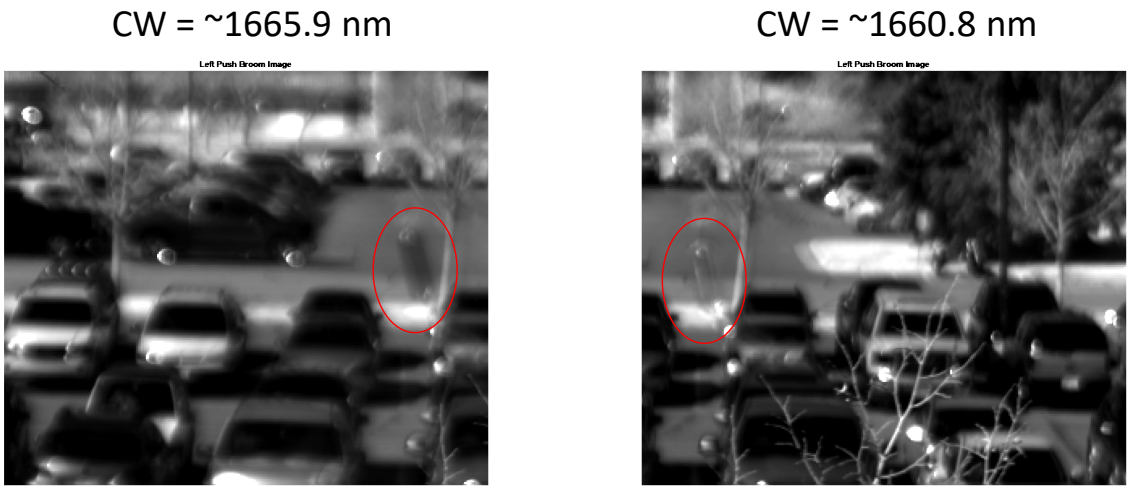

Fig. 1.7: Two "push broom" images from the FINIS instrument

The aerial test of the FINIS instrument during the second round of funding revealed a parallax issue. As the instrument scanned the ground, the location of the plane changed enough that raised objects (trees, buildings, etc.) appeared to change as the perspective location of the instrument changed. The variations in pixel intensities due to parallax was greater than the variations caused by the presence of CH_4, making it impossible to distinguish CH_4 leaks. An example is shown in Fig. 1.8. To solve this issue, the new FINIS instrument will use two sets of cameras and optics with the narrow-band filters tilted opposite of each other. This will enable the instrument to take simultaneous measurements in the absorption and transmission bands [5].

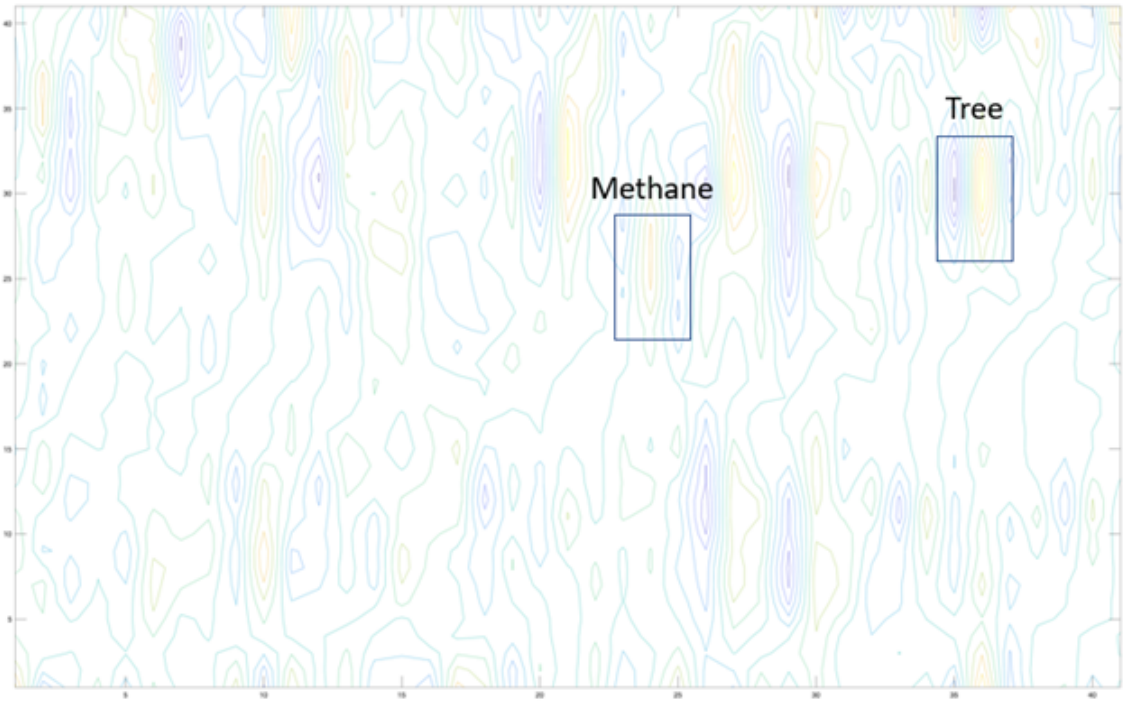

Fig. 1.8: "Contour map created by overlaying the absorption band data on top of the transmission band data and looking at the ratio between them. The difference between a variation in pixel intensities due to the presence of CH_4 and due to parallax from a tree are shown." [5]

FINIS is expected to have a spatial resolution of 125 m and a swath of 64 km, putting it in the mid range between an area flux mapper and a point source imager. The expected sensitivity is 12 ppb. The FINIS instrument is very small, lightweight, and power efficient (0.002 m^3, 1 kg, 5 W).

1.6 Comparison of CH_4 Instruments

A summary of the instruments is given in Table 1.1. Of the five major CH_4 missions discussed (other than FINIS), three of them can be classified as area flux mappers and two of them as point source imagers. FINIS' spatial resolution puts it as a mid range between the two categories. The 125 m spatial resolution is small enough to locate leaks to an area about the size of a football field, while the swath is still large enough to cover cities. Most of

the instruments are large, heavy, and power hungry making them less cost effective. FINIS and GHGSat are the most economical in terms of size, mass, and power, with FINIS ranking as the smallest, lightest, and least power consuming instrument.

Table 1.1: SWIR Satellite Sensor Comparison [8, 10–13]

Instrument	SCIAMACHY	TROPOMI	GOSAT-2	PRISMA	GHGSat-C2	FINIS (Expected)
Launch Year	2002	2017	2018	2019	2021	2024
Sensitivity (ppb)	30	12	5	60	19	54
Resolution (km)	30	7	10	0.03	0.025	0.125
Swath (km)	960	2600	1000	30	12	64
Size (m^3)	0.7	0.68	0.8	0.35	0.004	0.002
Mass (kg)	198	220	137	90	9	1
Power (W)	122	170	350	110	45	5

CHAPTER 2

SCIENCE

To better understand how the FINIS instrument works and why certain design choices were made, a basic background in absorption spectroscopy and its related technologies is needed. This chapter discusses the science behind absorption spectroscopy, the gases in the spectrum FINIS will be observing, and the effect of tilting an interference filter.

2.1 Absorption Spectroscopy

Absorption spectroscopy is the scientific method of differentiating materials based on the spectra of wavelengths they absorb or transmit. It can be used to determine temperature, composition, and motion of objects. Each particle of light, or photon, has a specific energy which corresponds to its wavelength. When photons strike an object they are either absorbed, transmitted, or reflected based on the photon's energy (or wavelength) and the composition of the material they impact. Analysis of the spectra of light coming from an object can reveal the material and its concentration [14]. An example of the absorption phenomenon in the atmosphere is shown in Figure 2.1.

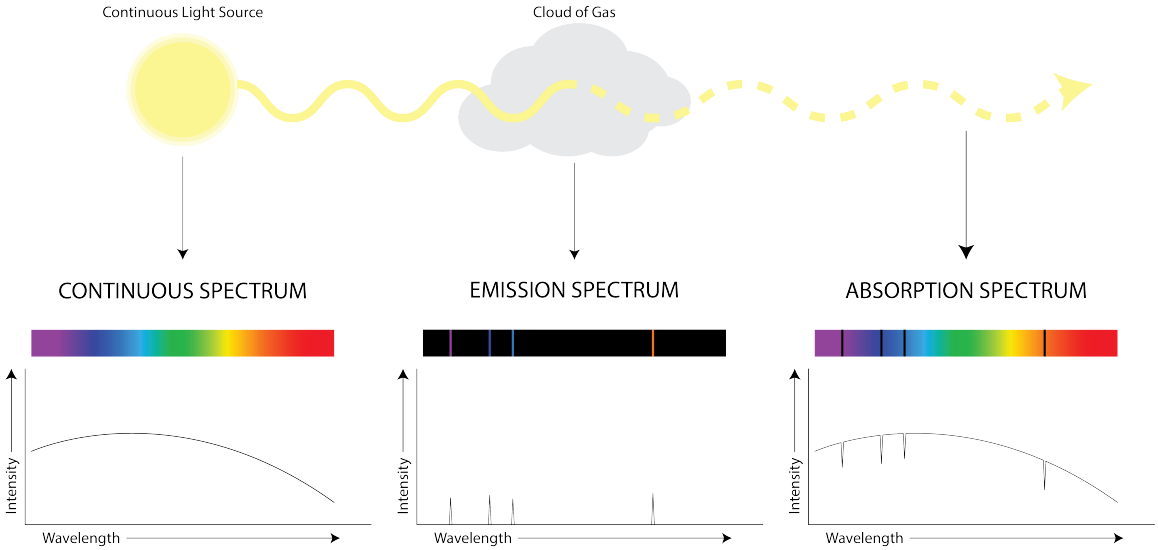

Fig. 2.1: Continuous light from the sun shines through a cloud of gas. Before the light passes through the cloud, the light is composed of a continuous spectrum. As the photons of light pass through the gas cloud, photons with energy levels equal to the excitation energies of the gas molecules are absorbed. The resulting light after the cloud of gas is the continuous spectrum minus the concentration of photons absorbed by the gas (the emission spectrum).

Methods for observing absorption spectra include prisms, diffraction gratings, Fabry Perot interferometers, and tilted interference filters. FINIS uses a tilted interference filter as its spectrometry method due to its advantages in narrow spectral resolution, mass, and size. More information on how tilted interference filters are used as spectrometers is given in section 2.3

2.2 Gases in the CH_4 Absorption Band

The 1.666µm absorption feature also has elements of H_2O that overlap the CH_4 absorption lines, so a wider spectral band must be observed to distinguish contributions from each component. FINIS accomplishes this by using a tilted interference filter to create a 10 nm wide spectral window and then uses Differential Optical Absorption Spectroscopy (DOAS) to estimate the concentration of each component.

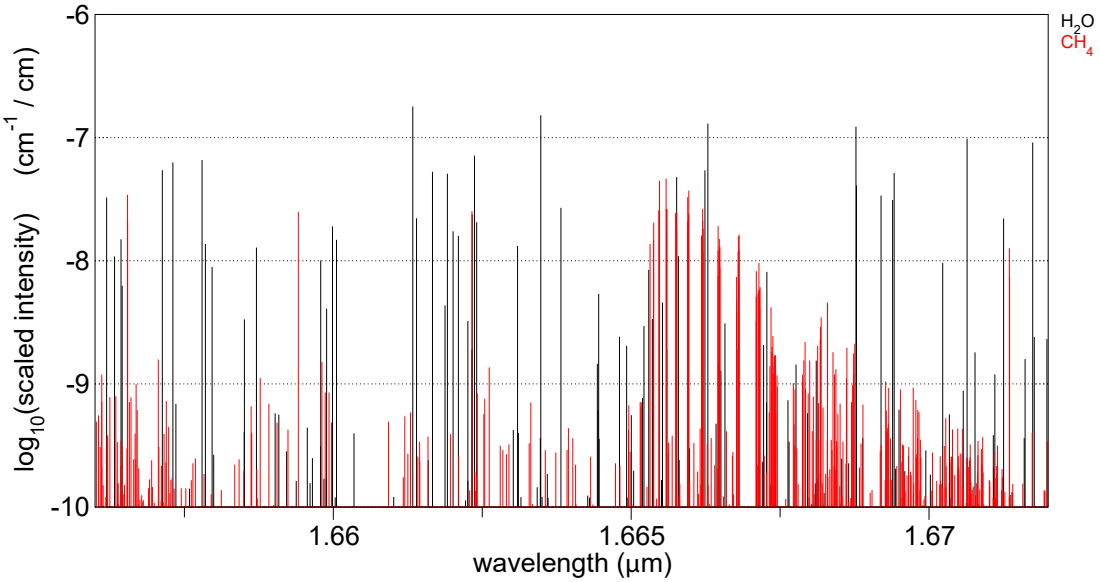

Fig. 2.2: CH_4 and H_2O absorption bands from Hitran 2004 data [15]

2.3 Tilted Interference Filter

Interference filters are made of thin dielectric coatings of varying refractive indices to create constructive and destructive interference patterns. As light passes through the filter it changes direction due to the differences between the refractive indices of the dielectric coatings. Depending on the wavelength, the light can either be transmitted, reflected, or absorbed by the filter [16]. Advances in interference filter technology have made it possible to manufacture filters with transmission as high as 98%, center wavelength (CWL) tolerances as low as 0.05 nm, and full width half maximum (FWHM) bandwidths as low as 0.1 nm [17].

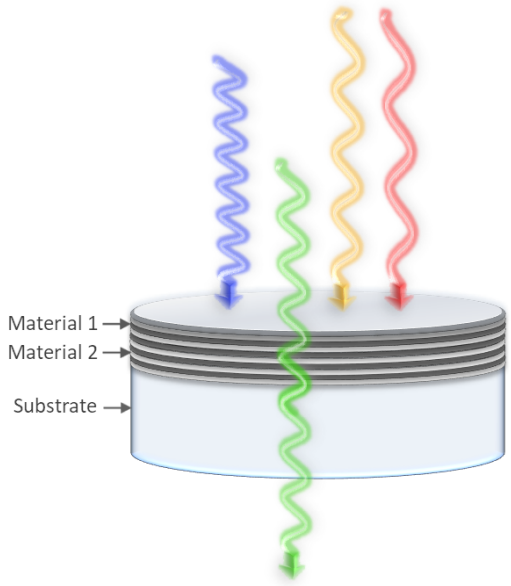

Fig. 2.3: Interference filters use thin layer dielectric materials to block all but a desired spectrum from transmitting.

As an interference filter is tilted away from normal incidence, the transmission spectrum is shifted to shorter wavelengths. This has the advantage of having a broader spectrum across the focal array, while keeping a narrow spectral resolution at each wavelength. The relation between angle of incidence (AOI) and CWL for collimated light at relatively small angles of incidence is show in Equation 2.1 [18].

$$\lambda_\theta = \lambda_o \sqrt{1 - \left(\frac{n_o}{n_{eff}} \sin\theta \right)^2} \tag{2.1}$$

Where:

- λ_θ = wavelength corresponding to the feature of interest at incident angle θ
- λ_o = wavelength corresponding to the feature of interest at normal incidence
- n_o = refractive index of incident medium
- n_{eff} = effective refractive index of the optical filter

- θ = angle of incidence

The FINIS interference filter will be tilted 10°, and with a FOV of 9° the effective spectrum on the focal area is 1657-1670 nm (AOI's between 5.5° and 14.5°). A simulation of how the angle of incidence (AOI) affects the CWL across the FINIS interference filter is shown in Figure 2.4.

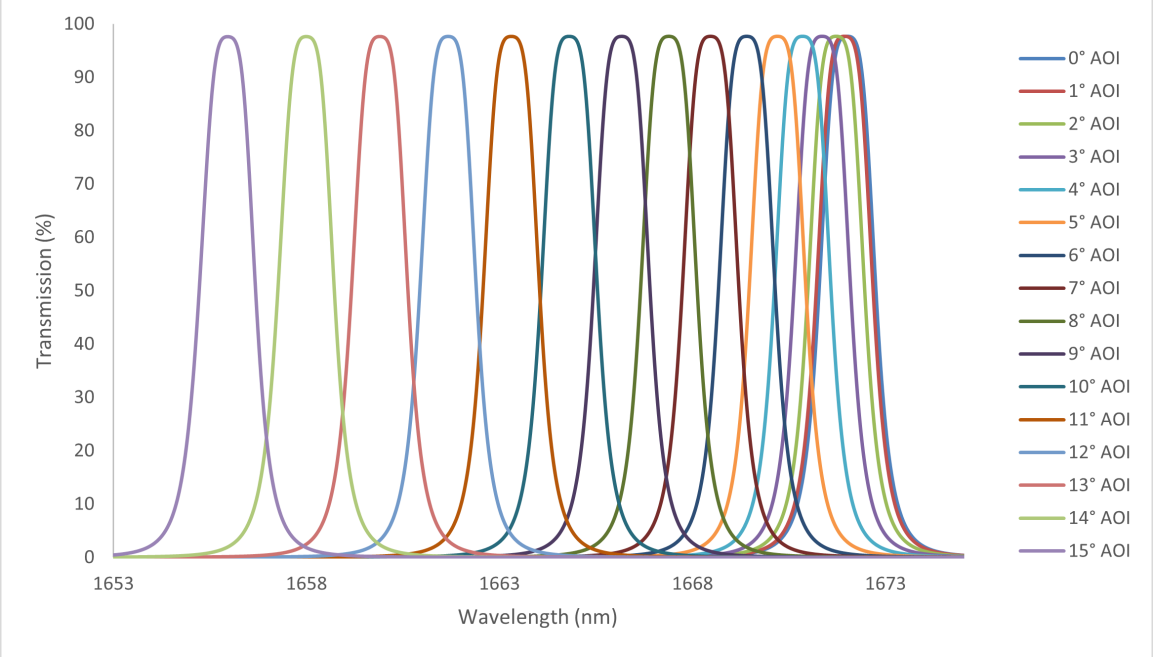

Fig. 2.4: Center wavelength shift for varying angle of incidence across the interference filter

CHAPTER 3

INSTRUMENT DESIGN PROCESS

This chapter provides a detailed analysis of the development of the FINIS instrument design including component selections, mechanism functions, analysis, and interfacing.

3.1 Original Instrument Design

The original FINIS instrument has a folded optical path with each lens mounted individually on an optical bench. The IR camera is a Goldeye CL-008 from Allied Vision and there are two context cameras and an IMU for positioning. The system also has a simple solenoid shutter.

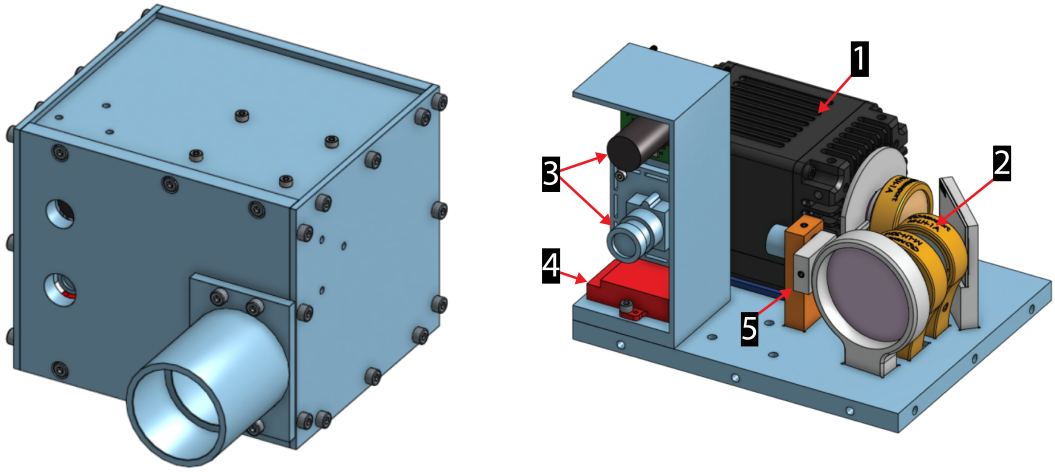

Fig. 3.1: Original FINIS CAD: (1) Goldeye Camera (2) Optics (3) Context Cameras (4) IMU (5) Shutter

The optical layout for the system was designed by Dr. Alan Marchant and consists of four COTS lenses, an out of band (OOB) filter, and an interference filter. A fold mirror is used

between L2 and L3 to allow the camera to be perpendicular to the aperture of the optics, creating a more compact footprint.

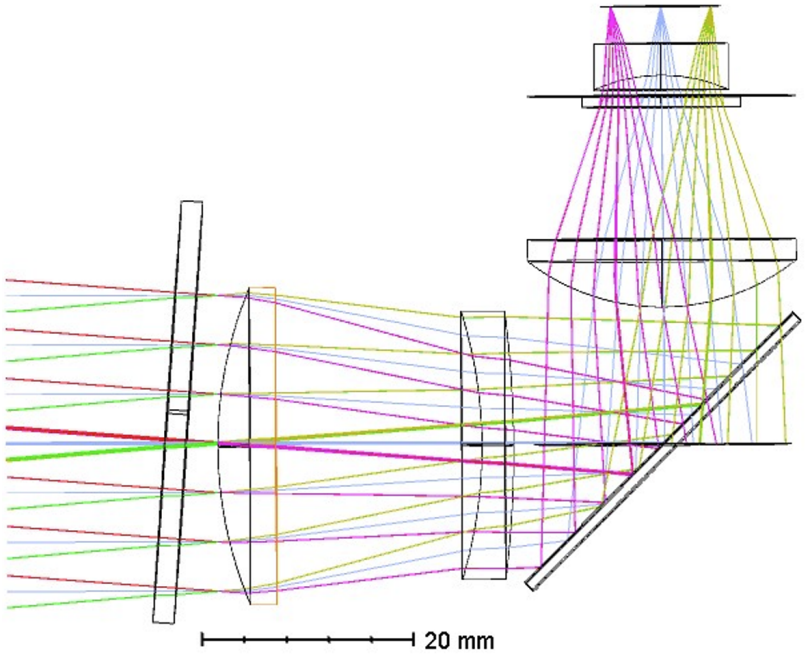

Fig. 3.2: Raytrace for the original FINIS optics

3.2 Camera Selection

The first step in the design process for the new FINIS instrument was to select the IR camera. The FINIS camera needs to be sensitive to incoming radiation at 1666 nm, be temperature stabilized, have a high pixel capacity, low readout noise, high quantum efficiency (QE), low dark current, and if possible make use of existing engineering. Several cameras options were explored with some of the options shown in Table 3.1.

Table 3.1: SWIR camera options

Manufacturer	Model	FPA	Pitch μm	Volume (mm^3)	Mass (g)	Interface	QE (%)
Allied Vision	Goldeye CL008	320x256	30	78x55x55	340	CameraLink	46
ArtRay	ArtCam-008TNIR	320x256	30	72x62x52	250	USB-2	60
First Light	C-RED-2	640x512	15	140x75x55	460	USB-3	65
FLIR	Tau SWIR	640x512	15	38x38x36	81	CameraLink	65
Hamamatsu	C14041-10U	320x256	20	56x56x98	520	USB-3	60
Hamamatsu	C12741-03	640x512	20	56x56x98	520	USB-3	60
Hamamatsu	C10633-13	320x256	30	50x50x55	225	USB-2	88
ICI	SWIR 640 P	640x512	15	56x56x98	130	USB-3	40
Jena	IK1513	320x256	30	91x91x86	850	USB-2	58
NIT	NSC1201-Si	640x512	15	49x49x33	125	USB-3	70
NIT	SenS-640	640x512	15	46x46x65	215	USB-3	70
Photon Focus	MV3-D640I-G2	640x512	15	60x60x61	265	Gig-E	58
Raptor	OWL 640	640x512	15	50x50x82	282	CameraLink	78
Raptor	OWL 320	640x512	30	50x50x70	250	CameraLink	78
SUI	320CSX	320x256	12.5	32x32x28	60	CameraLink	50
SUI	640CSX	640x512	12.5	32x32x28	45	CameraLink	50
SUI	320KTS-1.7RT	320x256	25	53x53x65	270	CameraLink	60
Xenics	XSW-320	320x256	20	43x45x51	129	CameraLink	63
Xenics	Cheetah 640CL	640x512	20	140x135x90	2000	CameraLink	63

A decision matrix is used to help narrow the camera selection. The weighting factors are the number of pixels, pixel pitch, sensor area, volume, mass, camera interface, and QE. The volume and sensor area are weighted as the most important factors, followed by the QE and

mass. The number of pixels, pitch, and camera interface are important, but not weighted as high as the other factors. To make use of prior engineering, the sensor size should be the same as the previous camera. The preferred interface is ethernet (Gig-E) or cameralink.

Table 3.2: SWIR decision matrix

		# of Pixels	Pitch	Sensor Area	Volume	Mass	Interface	QE (%)	Score
Weighting Factor		3	3	8	8	5	4	6	
Allied Vision	Goldeye CL008	2.5	10	10	1.2	1.3	7	5.2	193
ArtRay	ArtCam-008TNIR	2.5	10	10	1.2	1.8	1	6.8	181
First Light	C-RED-2	10	5	10	0.5	1	3	7.4	190
FLIR	Tau SWIR	10	5	10	5.5	5.6	7	7.4	269
Hamamatsu	C14041-10U	2.5	6.7	3	0.9	0.9	3	6.8	116
Hamamatsu	C12741-03	10	6.7	6	0.9	0.9	3	6.8	163
Hamamatsu	C10633-13	2.5	10	10	2.1	2	1	10	208
ICI	SWIR 640 P	10	5	10	0.9	3.5	3	4.5	189
Jena	IK1513	2.5	10	10	0.4	0.5	1	6.6	167
NIT	NSC1201-Si	10	5	10	3.6	3.6	3	8	232
NIT	SenS-640	10	5	10	2.1	2.1	3	8	212
Photon Focus	MV3-D640I-G2	10	5	10	1.3	1.7	10	6.6	223
Raptor	OWL 640	10	5	10	1.4	1.6	7	8.9	225
Raptor	OWL 320	10	10	10	1.6	1.8	7	8.9	243
SUI	320CSX	2.5	4.2	1	10	7.5	7	5.7	208
SUI	640CSX	10	4.2	3	10	10	7	5.7	259
SUI	320KTS-1.7RT	2.5	8.3	3	1.6	1.7	7	6.8	146
Xenics	XSW-320	2.5	6.7	2	2.9	3.5	7	7.2	155
Xenics	Cheetah 640CL	10	6.7	6	0.2	0.2	7	7.2	171

The decision matrix shows that the Flir Tau SWIR is the best camera option for the FINIS system. The Tau SWIR is very small and lightweight, with low dark current and read noise. As another advantage, OSS has used the Tau SWIR on previous missions so their software and electrical engineering work can be reused on FINIS.

3.3 Design Iterations

With the camera selected, the next step in the design process was deciding the optical layout. As mentioned in Section 1.5, the new FINIS instrument will have two cameras with separate optical paths. After FINIS' second round of funding a design was developed with the same optical layout as developed by Alan Marchant, but with the second camera system opposite of the first (see Fig 3.3). The design was very inefficient and subsequent iterations removed the fold mirror to allow for a straight optical path (Examples in Fig 3.4.

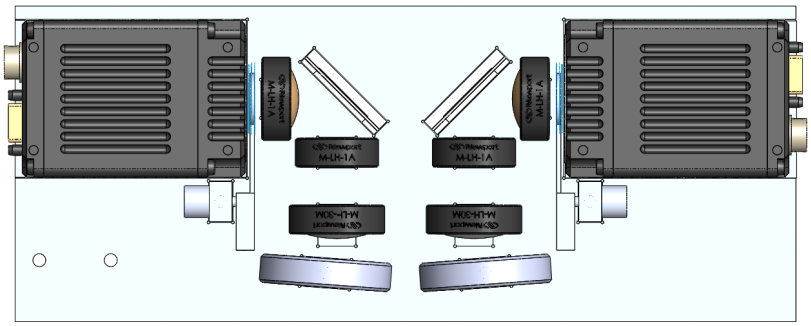

Fig. 3.3: Two camera FINIS system with a folded optical path

Several iterations were needed to optimize the instrument design as new information was obtained. A summary of the iterations is given below:

- Rev 1 and 2: The Goldeye camera is replaced with the Flir Tau SWIR and the fold mirror is removed in favor of a straight optical path. The optical components are mounted with the same style of mounts as the original FINIS design. The shutter arm is elongated to cover the apertures of both cameras.
- Rev 3: A lens tube approach is used to mount the optical components. At this point

in the design, a single COTS lens tube holds all the lenses, with the idea that adapter mounts will be built for each lens to screw into the main tube. A larger aperture was implemented to give a higher signal to noise ratio. During this revision several shutter designs were investigated. The final shutter design during this revision is a single mount in between the cameras with two solenoid actuators.

- Rev 4: The lens tube is refined to minimize size and mass. Each lens is held by a custom piece of the lens tube and the front piece mounts to the optical bench. The interference filter is changed back to 40mm as changing optics for a larger aperture is not reasonable. The shutter is removed from the design due to concerns from OSS about risks from adding a moving mechanism.
- Rev 5: The custom lens tube pieces are replaced with COTS lens tubes to reduce instrument costs. The only custom piece is the mount for the interference filter.
- Rev 6: The L4 Mount is switched from COTS components to a custom piece because the COTS components obstructed the optical path. The interference filter mount is also changed to reduce the number of lens tube components and simplify the mounting method.
- Rev 7: The lens tube components are simplified further to reduce the number of pieces.
- Rev 8: The tilt of the interference filter is changed from 4 degrees to 10 degrees to provide a wider spectrum.
- Rev 9: Discussions with members of The Aerospace Corporation who have flown the Tau SWIR camera reveal that random hot pixels were common on the instrument sensor. As a result of the conversations, a shutter is added back to the instrument design to allow for onboard calibrations. The shutter is split into two mechanisms on either side of the instrument.
- Rev 10: The shutters are moved in between the lens tubes but offset from each other.

- Rev 11: The shutters are combined into a single shutter plane. A slot is cut into the optical bench to accommodate when the shutter is in the "open" position. A baffle is also implemented to prevent stray light from entering the lens tubes.
- Rev 12: Holes are added to the lens tubes to radially mount infrared LEDs. The LEDs will act as a calibration source while in orbit. As a result, the shutter is moved further along the optical path.
- Rev 13: The calibration source is changed from radially mounted LEDs on the lens tube to LEDs mounted on a circuit board inside the lens tubes. The shutter is moved back to its location after L3, and the shutter protrusion on the baffle is removed to allow the FPGA board to be mounted on top of the baffle.
- Rev 14: Analysis from John Noto reveals that the optical focus of the instrument is incorrect. An attempt is made to fix it by increasing the distance between L4 and the instrument sensor.
- Rev 15: Information from Brandstrom Instruments reveals that the solenoid is not strong enough to hold the shutter in place during launch vibrations. A pin puller from EBAD is implemented to hold the shutter.
- Rev 16: More optical analysis from John Noto reveals the correct distance between L4 and the instrument sensor. The optics are moved closer to the detector and the lens tube components are adjusted to accommodate the changes.
- Rev 17: The EBAD pin puller is switched to a nano pin puller from DCubed. The new pin puller is situated between the lens tubes instead of between the cameras and is fully resettable after actuation.

A few of the major design changes are shown in Fig 3.4. See Appendix A for images of the other design iterations.

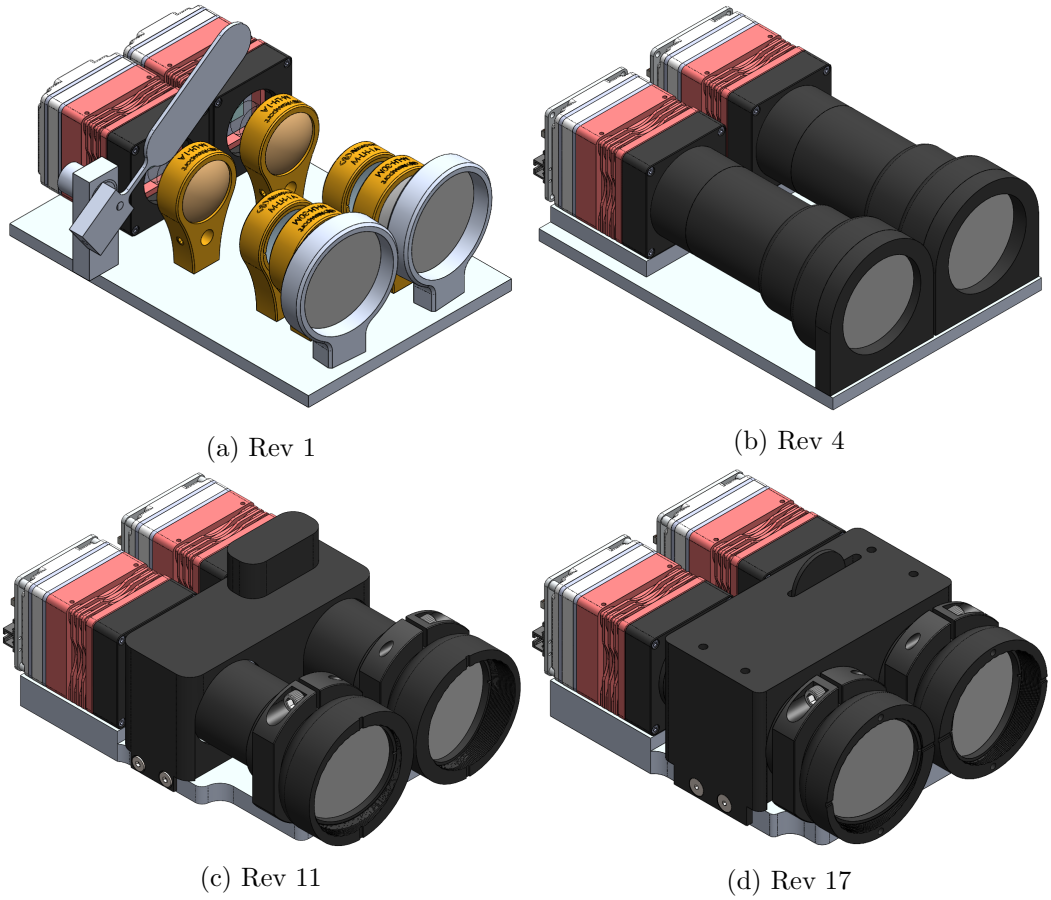

(a) Rev 1

(b) Rev 4

(c) Rev 11

(d) Rev 17

Fig. 3.4: A few iterations of the FINIS design

The shutter is the component with the most design iterations (See Fig 3.5). The first design (a) implemented a single long arm shutter for both cameras. This design wasn't optimal because the shutter arm extended too high when in the open configuration. The next iteration (b) took a new approach of putting the shutter mount in between the cameras. Two solenoids are mounted on the same block, which slightly increased the distance between the cameras. However, this design neglects that the solenoid works best when the shutter's center of mass is aligned with the center of rotation. Without centering the shutter mass about the rotation the lifetime of the solenoid would be reduced. Therefore, the next design (c) split the shutters to either side of the cameras. The height when open is greatly reduced compared to design "a", but the overall width of the instrument is increased. In design

"d" the shutters are moved back between the cameras but offset from each other along the optical axis. This design requires a longer baffle to cover the shutters and presents potential differences in the optical paths for the two cameras. Finally, design "e" combines the shutters into a single equally balanced shutter plane acting as the shutter for both camera systems. A slot is cut in the optical bench to accommodate the lower side of the shutter when in the open position, reducing the overall height. The final shutter design is discussed more in Section 4.4.

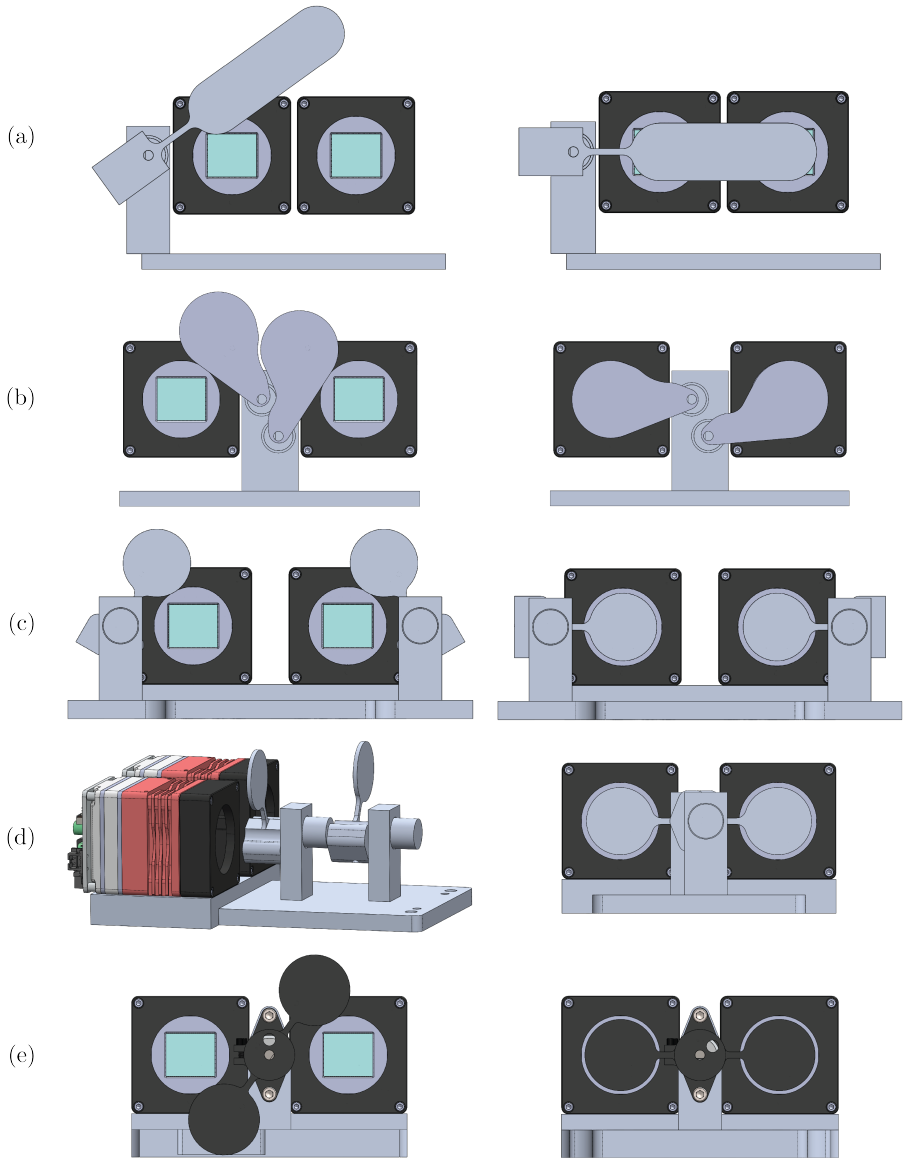

Fig. 3.5: Shutter design iterations

CHAPTER 4

FINAL DESIGN AND COMPONENT ANALYSIS

This chapter provides an overview of the final FINIS instrument design and an analysis of the components used. The main components in the system are the Tau SWIR InGaAs cameras, lens tubes, tilted interference filters, and calibration mechanisms for flat field and dark current measurements. The instrument SWaP are 140x89x66 mm^3, 804 g, and 5 W.

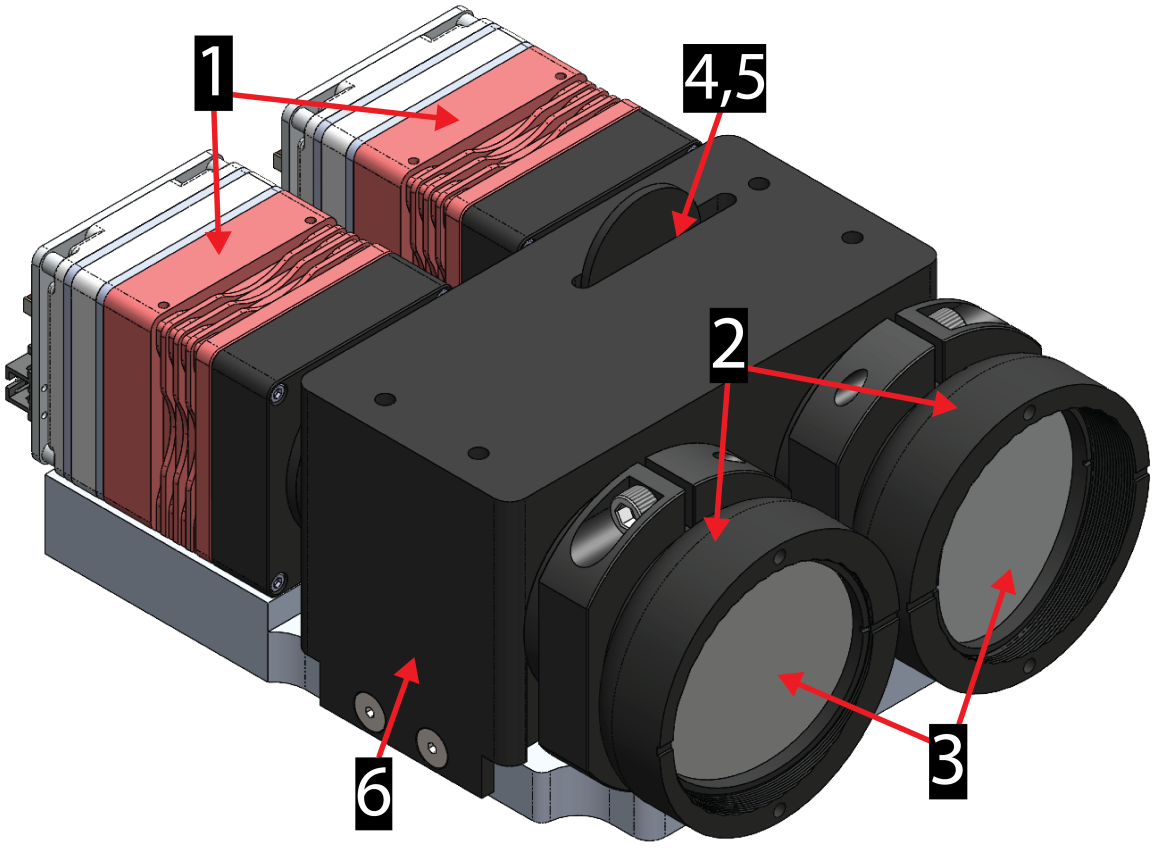

Fig. 4.1: FINIS Instrument (1) Tau SWIR Cameras (2) Lens Tubes (3) Tilted Interference Filters (4) Shutter mechanism 5) Infrared calibration source (6) Baffle

4.1 Optical Design

The FINIS optical layout is a simple variation of the design made by Alan Marchant, with the major change being the removal of the fold mirror to create a straight optical path. The lenses are all COTS components from Thorlabs and they have AR coatings to prevent reflections in the 1050-1700 nm region. The interference filter doesn't block all of the shorter wavelengths equally, so an out of band (OOB) filter is used to block anything below 1550 nm.

Initial analysis was performed in a student version of a raytrace software called Oslo to verify that the straight optical path worked as expected. John Noto from OSS has helped enter the design into Zemax to verify the focus and estimate the point spread function (PSF) of the instrument. The FOV of the instrument is 9° with a focal length of 62 mm, aperture of 28 mm, and F/# of 2.2. The resulting GSD is 125 m and the swath is 80 km. The current raytrace is shown below.

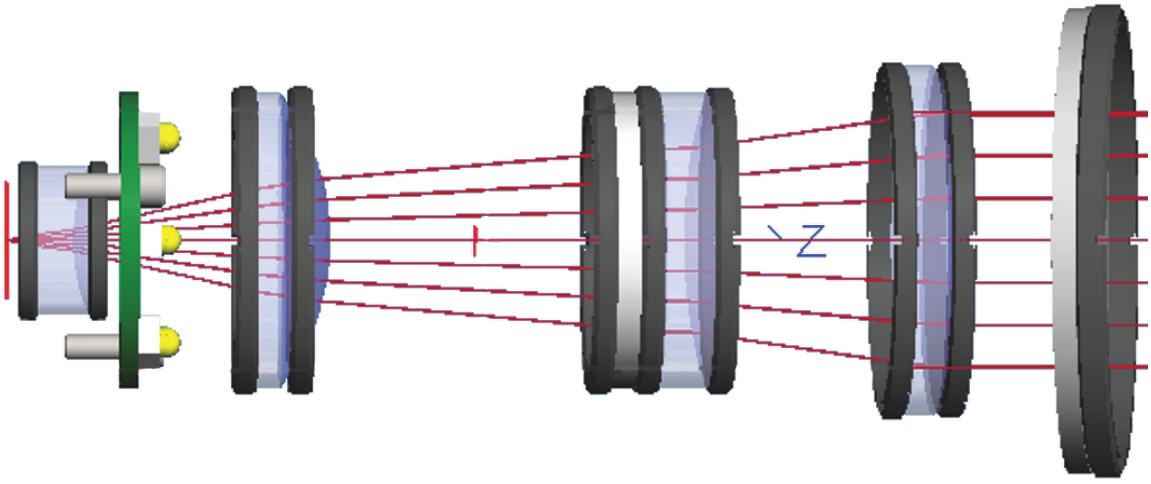

Fig. 4.2: Raytrace of the FINIS optics with 0° AOI light.

4.2 Interference Filter

Advances in interference filter manufacturing technologies have made it possible to improve the filter specifications. The original design for the interference filter had a CWL of

1666.3±0.75 nm, FWHM of 2±0.7 nm, and peak transmission of >50%. The new design has a CWL of 1672±0.25 nm, FHWM of 1.5±0.25 nm, and peak transmission of ∼98%. The tighter FWHM will give the instrument greater spectral resolution, and the increase in transmission greatly increases the SNR. The change in CWL for the new filter is driven by the filter tilt change from 4° to 10°. The resulting spectrum on the FPA is 1658 to 1668 nm.

Figure 4.3 shows how the filter tilt impacts the CWL across the FPA. The CH_4 absorption band is mapped on one side of the FPA, and it transitions to the transmission band on the other side of the FPA. As the satellite scans the ground, each ground point is observed at the full spectrum of wavelengths.

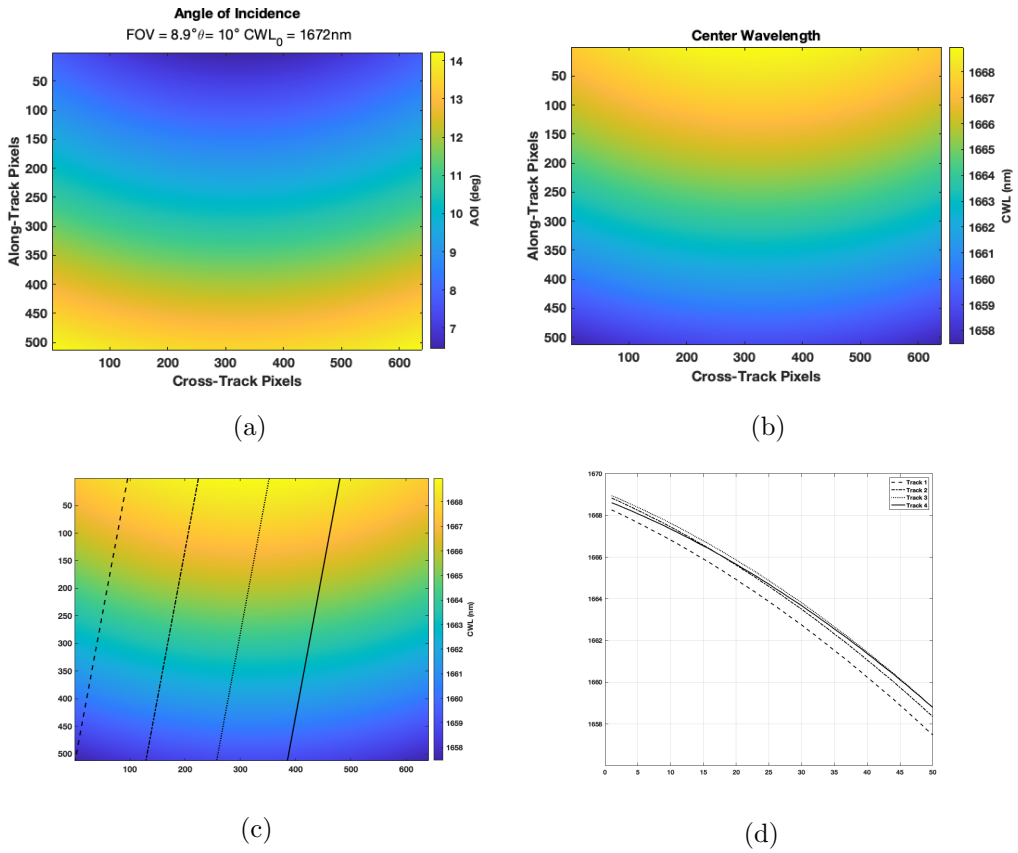

Fig. 4.3: Plot "a" shows how the AOI on the interference filter is mapped on the FPA, and "b" shows the corresponding wavelengths. Plot "c" shows how four different ground locations are tracked across the FPA during an overpass, and the observed wavelength for each point is shown in plot "d".

FINIS employs two camera systems with filters at opposite tilts, allowing each ground point to be observed in the absorption and transmission bands at the same time. This helps prevent any errors due to parallax and albedo changes, and provides greater accuracy in CH_4 concentration retrieval.

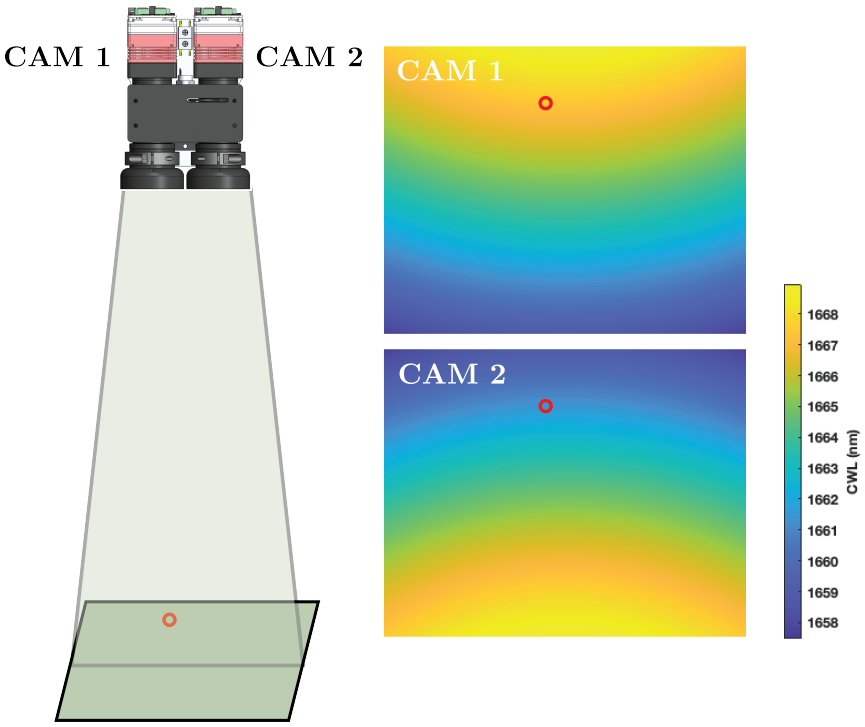

Fig. 4.4: The CAM1 and CAM2 interference filters are tilted opposite from each other, creating opposite spectrums across the focal array. This allows each ground location to be observed in the CH_4 absorption and transmission bands at the same time.

4.3 Lens Tube Components

The FINIS optics are composed of a series of lenses, an OOB filter, and an interference filter. The majority of the lens tube components are COTS, with the exception of the mounts for L4 and the interference filter. The infrared calibration source is attached to the L4 mount inside of the lens tube.

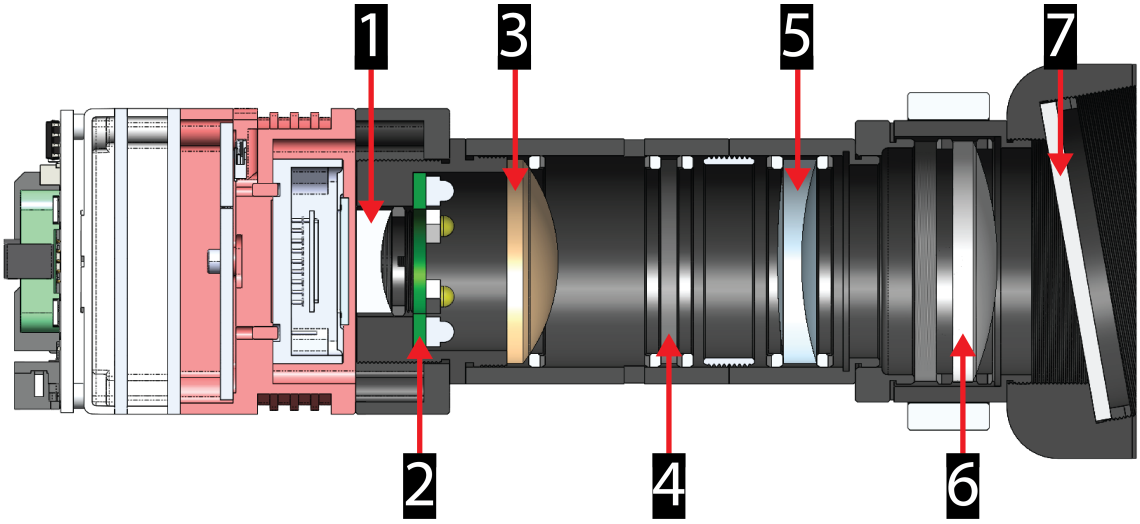

Fig. 4.5: Cross-section of optics (1) L4, Plano Concave Lens (2) Infrared Calibration Source (3) L3, Plano Convex Lens (4) OOB Filter (5) L2, Negative Meniscus Lens (6) L1, Plano Convex Lens (7) Interference Filter

Spanner wrenches with measurement marks are used to install each of the lenses to the correct locations. Before spacecraft integration, each of the retaining rings are secured with loctite to ensure they don't move during launch vibrations. The exploded view in Figure 4.6 shows how the lens tube components relate to each other. The interference filter mount needs precise clocking to ensure the filter is tilted in the right direction. Upon initial assembly, the face of the adjoining part is ground until the clocking is correct.

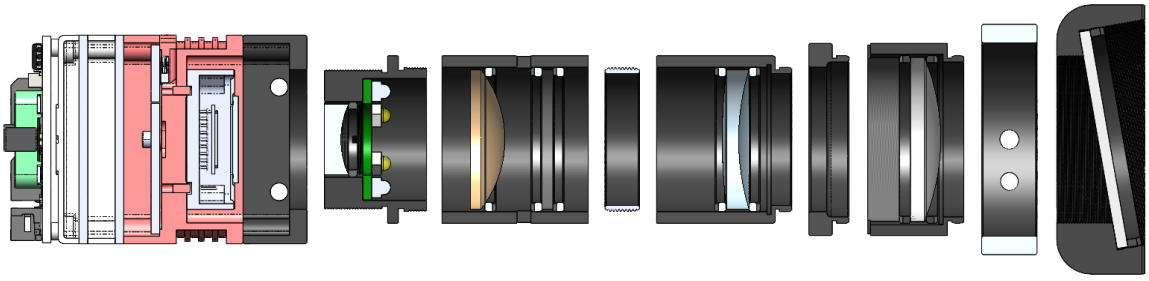

Fig. 4.6: Exploded view of lens tube components

4.4 Shutter

Implementation of a shutter is necessary for on-board calibration of dark current prior to data acquisitions. The shutter is required to be low risk and easy to control, and shouldn't overly increase the size of the FINIS instrument. To address the issues of risk and controllability, a 55° self-restoring solenoid will be used rather than a motor. The solenoid is magnetically latched in its home position until energized, and then rotates to its secondary position until power is removed. Even in the event of an electrical failure, the shutter will fail in its open position and will not inhibit data acquisition. The solenoid is quoted to operate reliably for 2.5 million cycles. At one calibration per orbit, the shutter will only be actuated about 6000 times per year leaving plenty of margin.

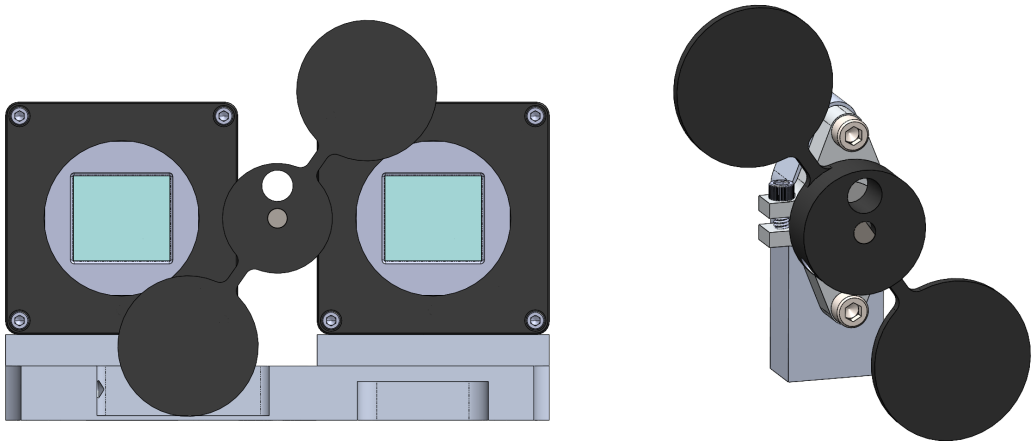

Fig. 4.7: Final shutter design

The holding torque of the solenoid is only 6 grams, so a mechanism is needed to prevent the shutter from rotating during launch vibrations. The solution used for this design is a pin puller that holds the shutter in an "open" position. The selected pin puller is the ND3PP from DCubed [19]. The pin puller is TRL 9 and is fully resettable when used in lab testing. Once in orbit, a current is applied to the pin puller and the plunger mechanism retracts and the shutter is free to perform its rotations.

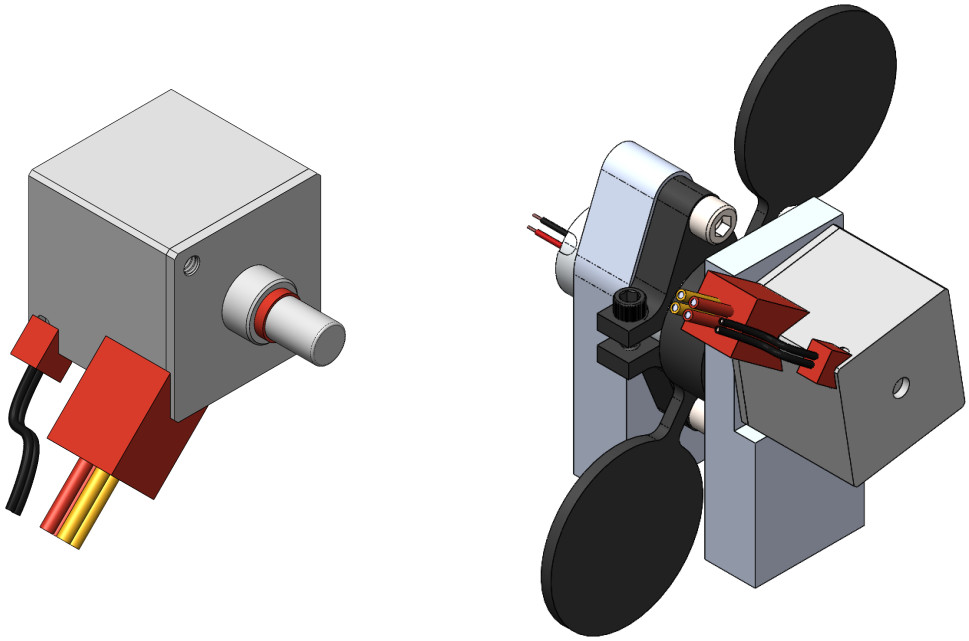

Fig. 4.8: ND3PP nano pin puller from DCubed. The pin puller is used to hold the shutter during launch.

The solenoid is quoted to last 2.5 million cycles.

4.5 Infrared Calibration Source

An infrared calibration source is implemented in the design to allow for on-board flat field and radiometric calibrations. A more detailed overview of the calibration process is given in chapter 6, but a brief design overview is given here.

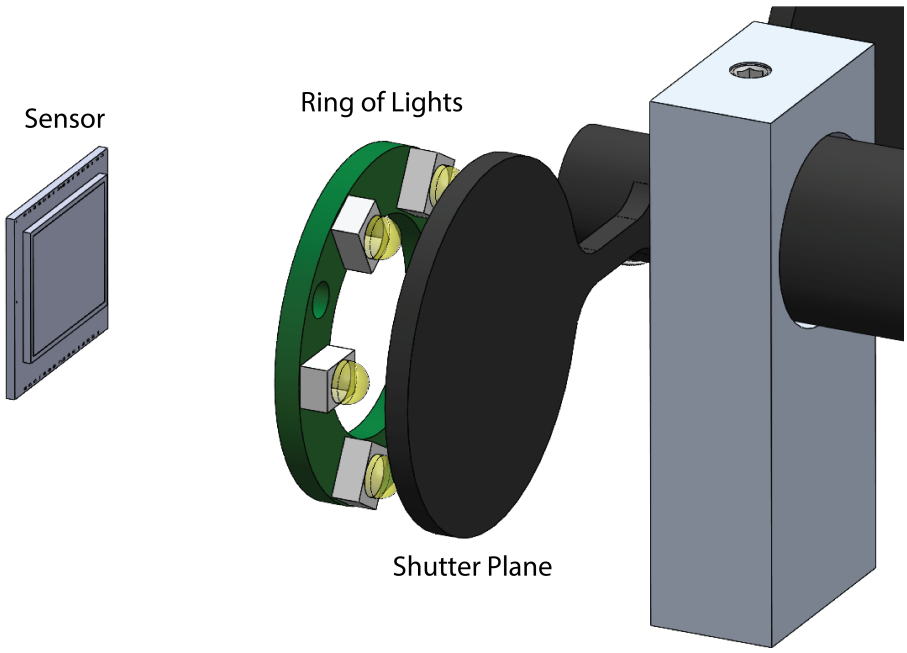

Fig. 4.9: Infrared Calibration Source

The infrared calibration source consists of a ring of LEDs that emit radiation at 1650 nm. The infrared light shines onto a diffuse shutter plane to create a uniform emitter back to the camera sensor. The current to the LEDs can be set to different values for the data points in the radiometric calibration.

4.6 Alignment

The FINIS cameras need to be aligned parallel to each other for each pixel to match the corresponding ground location of the pixel on the opposite camera. At an altitude of 550 km, the cameras need to be aligned within five arc seconds for each pixel to match the corresponding pixel by 90 percent. This tolerance cannot be reasonably reached or measured, so the instrument will be aligned to best reasonable effort and then misalignments will be corrected in data processing.

To ensure the best alignment possible and for repeatability of assembly, alignment pins will be used for positioning the cameras. Two pins are used to align the c-mount attached to

the camera body and another pin is used to position the tube clamp at the end of the lens tube.

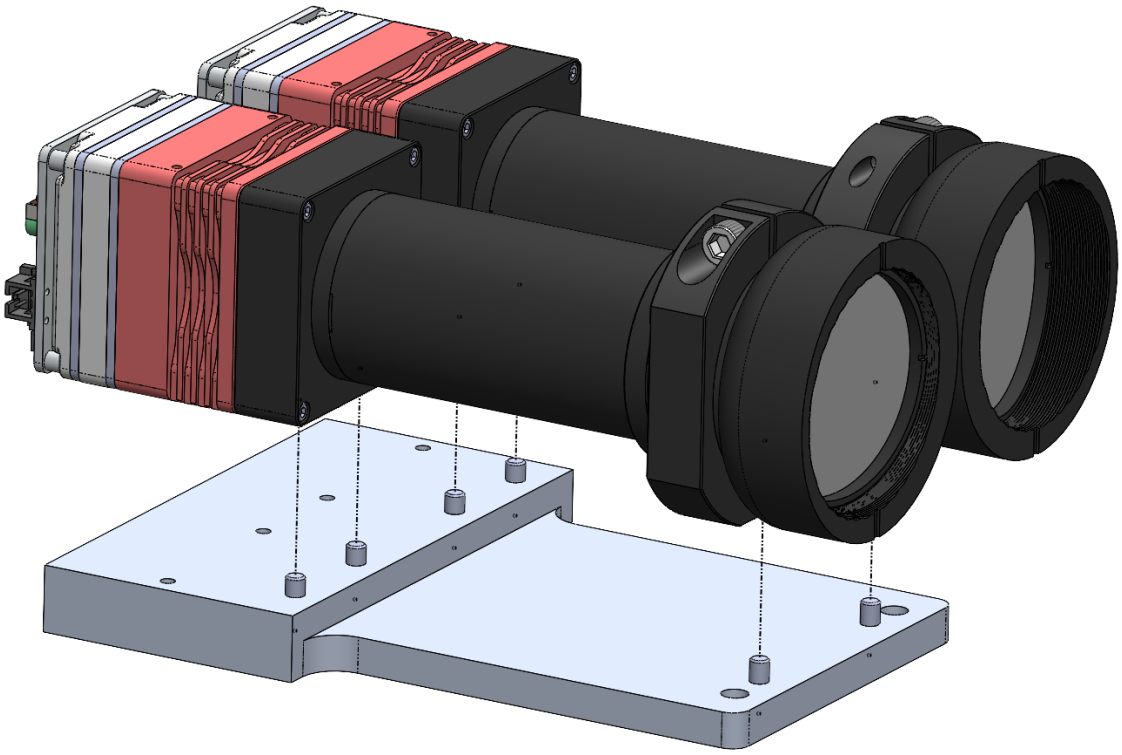

Fig. 4.10: Pins are used to align the FINIS cameras

4.7 Material Selection and Outgassing

This section will analyze the materials in the FINIS instrument and their outgassing characteristics. Outgassing is quantified by the percent Total Mass Loss (TML) and percent Collected Volatile Condensable Material (CVCM). The TML is the total mass of material that is outgassed from a test sample when maintained at a specific temperature and time. The CVCM is the quantity of outgassed matter from the test sample that is condensed and collected at a specific temperature and time. NASA requires that the TML be $\leq 1\%$ and the CVCM be $\leq 0.1\%$ for space applications [20]. All values are from the NASA GSFC outgassing data, unless otherwise specified. Materials not listed in the table are Aluminum 2024-T3, Aluminum 6061-T6, gold plated brass, gold plated phosphor bronze, type 303 SS,

and Remko B Iron.

Table 4.1: Material outgassing characteristics

Material	**Where Used**	**TML %**	**CVCM**
Aeroglaze Z306 Black Paint [21]	Baffle	1.0	0.02
Black Anodize Type II Class II	Lens tube components	0.75	.02
Fused Silica	Interference filter, OOB filter	NA	NA
N-BK7	Thorlabs Lenses	NA	NA
Diallyl Orthophthalate	JF connectors	0.42	0.00
Teflon (Virgin)	Solenoid	0.02	0.01
Ensinger Hyde PEEK 450G	Solenoid	0.30	0.02
3M 2216 BA Gray Epoxy Adhesive	Solenoid	0.99	0.02
3M Kapton 1205 Adhesive Tape	Solenoid	1.61	0.14
NEMA MW77-C Wire	Solenoid	NA	NA
Class 180 Copper Polyester-Imide	Solenoid	0.12	0.00
Teflon Insulated Wire per M16878	Solenoid	0.01	0.00
Alnico 8C	Solenoid	NA	NA
PA6T Resin [22]	LED	0.08	NA
Silicone Resin	LED	0.06	0.02
Polycarbonate	Diffuser	0.20	0.00
FR-4	PCB	0.32	0.01
Alodine 1132	Pin Puller	0.51	0.00
Fluoropolymer M23053/4-301-0	Pin Puller	0.12	0.04
Epoxy 6014123	Pin Puller	0.59	0.01
PolyEtherImide 6004202	Pin Puller	0.44	0.00

CHAPTER 5

INTERFACES

This chapter provides the mechanical and electrical interfaces of the FINIS instrument.

5.1 Mechanical Interface

The FINIS instrument interfaces with the ACMES spacecraft with four #8-32 holes on the bottom of the optical bench. The instrument is 140x89x66 mm^3 and weighs 804 g.

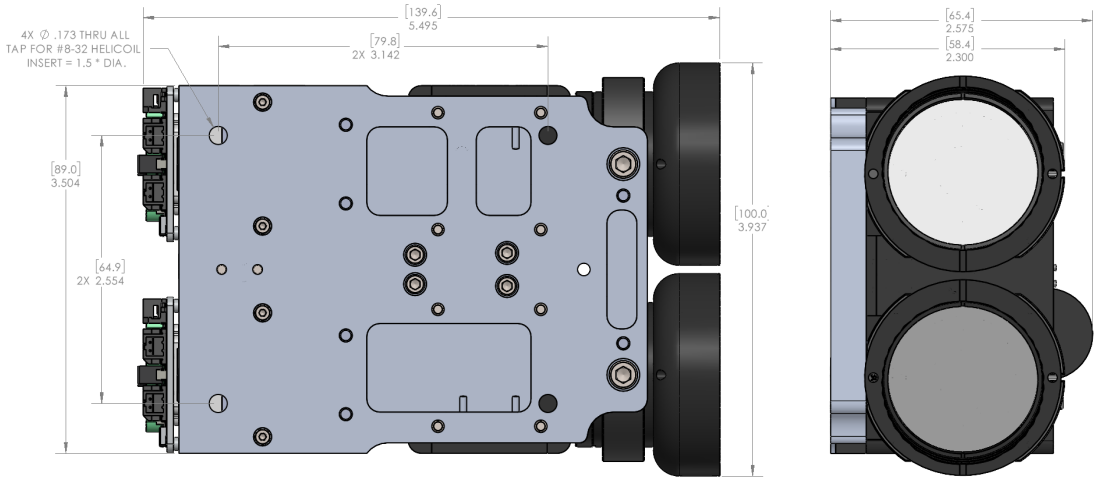

Fig. 5.1: Mechanical interface for the FINIS instrument

FINIS points out of the nadir side of the spacecraft and attaches to one of the side panels.

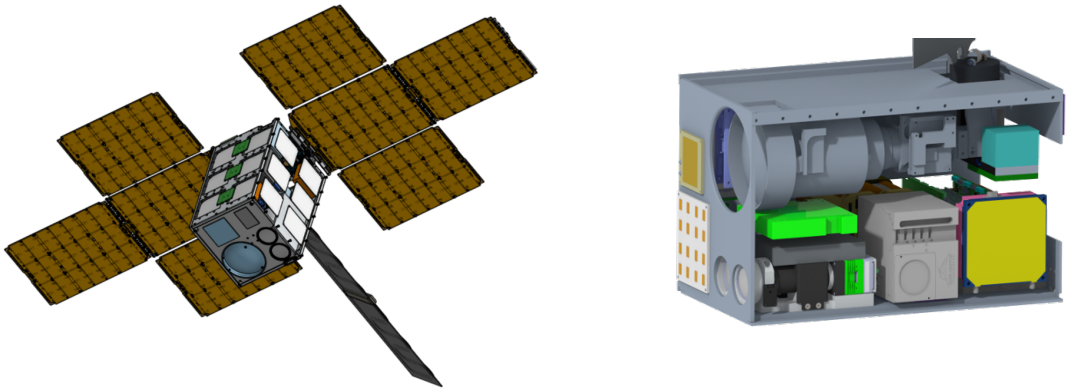

Fig. 5.2: FINIS inside the ACMES spacecraft

5.2 Electrical Interface

There are three electrical interfaces on the instrument, one each for the two Tau SWIR cameras and one for the calibration mechanisms. The interfaces for each of them will be discussed in the following subsections.

5.2.1 Tau SWIR Interface

The Tau SWIR cameras each have two electrical ports, a high-density 50-pin connector for data and controla and a TEC power connector.

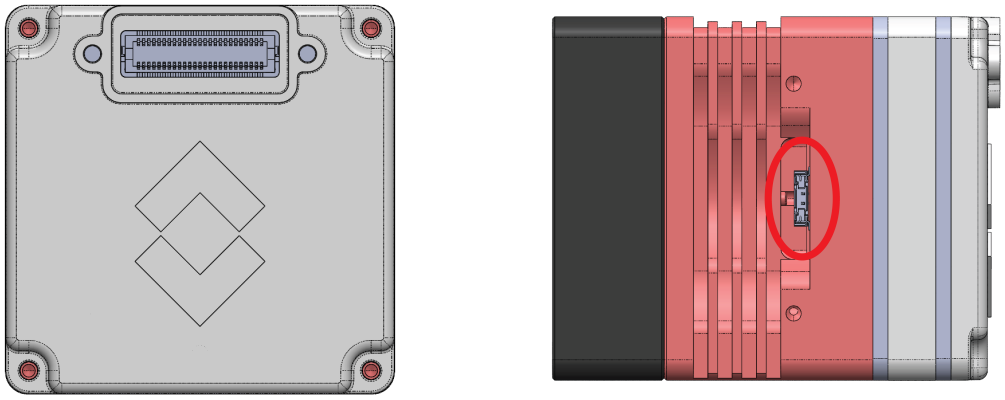

Fig. 5.3: Left: high-density 50-pin connector Right: TEC power connector

The pinout for the 50-pin connector is given below:

Pin #	Signal Name	Pin #	Signal Name
1	COMM_TX (RS232_TX_OUT)	2	COMM_RX (RS232_RX_IN)
3	CMOS LINE_VALID_OUT	4	CMOS FRAME_VALID_OUT
5	DGND	6	DGND
7	CAMLINK_CLK [P]	8	CAMLINK_CLK [N]
9	CAMLINK_DATA [0P]	10	CAMLINK_DATA [0N]
11	CAMLINK_DATA [1P]	12	CAMLINK_DATA [1N]
13	CAMLINK_DATA [2P]	14	CAMLINK_DATA [2N]
15	CAMLINK_DATA [3P]	16	CAMLINK_DATA [3N]
17	DGND	18	DGND
19	DISCRETE IO REG [0]	20	CMOS DATA_OUT [13]
21	EXTERNAL_SYNC	22	CMOS DATA_OUT [12]
23	CMOS DATA_OUT [11]	24	CMOS DATA_OUT [10]
25	CMOS DATA_OUT [9]	26	CMOS DATA_OUT [8]
27	DGND	28	DGND
29	CMOS DATA_OUT [7]	30	CMOS DATA_OUT [6]
31	CMOS DATA_OUT [5]	32	CMOS DATA_OUT [4]
33	CMOS DATA_OUT [3]	34	CMOS DATA_OUT [2]
35	CMOS DATA_OUT [1]	36	CMOS DATA_OUT [0]
37	DGND	38	DGND
39	CMOS CLOCK_OUT	40	Z
41	DGND	42	DGND
43	VID_OUT_H	44	VID_OUT_L
45	DGND	46	n/c
47	MAIN_PWR_RTN	48	MAIN_PWR
49	MAIN_PWR_RTN	50	MAIN_PWR

Fig. 5.4: Tau SWIR 50-pin connector pinout

A breakout board made by OSS will be used to interface with the Tau SWIR cameras. The board has connections for cameralink data interface, camera and TEC power, and three thermistors. The breakout board plugs into the 50 pin connector on the back of the camera and then has a jumper line that goes to the TEC power input.

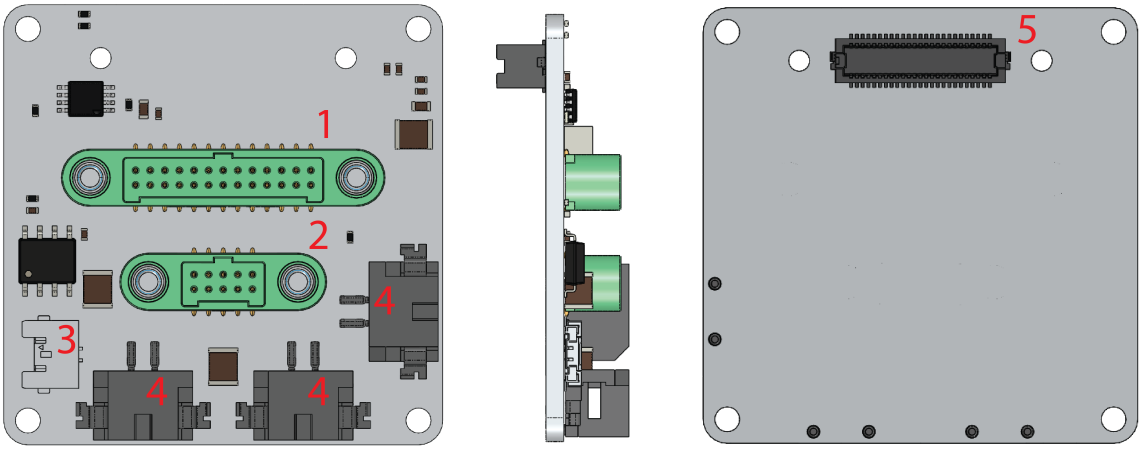

Fig. 5.5: Breakout board for Tau SWIR cameras (1) Cameralink Data Interface (2) Camera Power (in) (3) TEC Power (out) (4) Thermistor Connections (5) 50 Pin Connector Interface]

The schematic for the cameralink data interface and the camera power are given in Figure 5.6. See Appendix B for the full schematic.

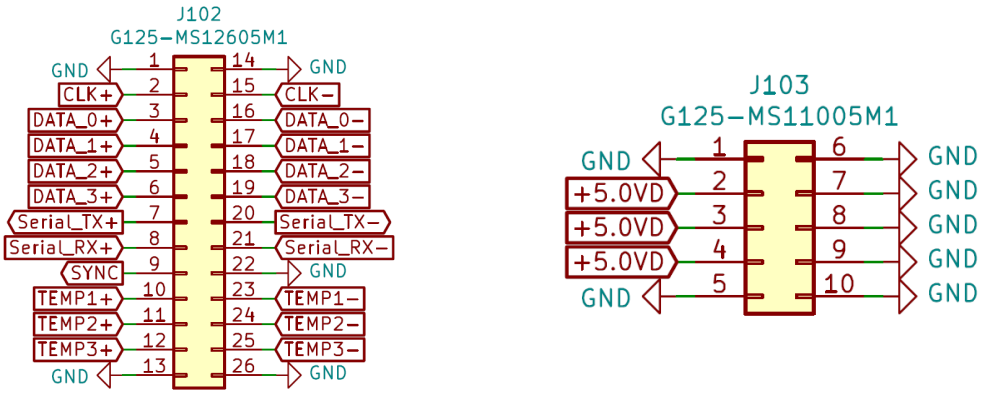

Fig. 5.6: Left: Cameralink schematic Right: Camera power schematic

The power input to the breakout board is 5V and on average consumes 2.3W per camera.

5.2.2 Calibration Mechanisms Interface

The calibration mechanisms include a solenoid, pin puller, and two boards with infrared LED's. Table 5.1 shows the power requirements for each mechanism.

Table 5.1: Calibration mechanism power requirements

	Solenoid	Pin Puller	LEDs
Voltage (V)	5	2	0.9
Resistance (Ω)	1	1.3	
Current (A)	0.19	2	0.05
Power (W)	0.93	4	.05

The calibration mechanisms are wired to four sets of winchester connectors for ease of assembly, and then the winchesters are soldered to a jumper that interfaces with a 10 pin connector on the FPGA.

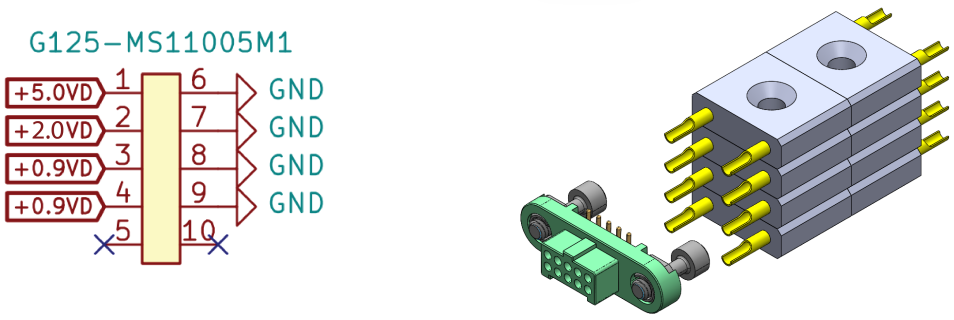

Fig. 5.7

CHAPTER 6

CALIBRATION

This chapter provides a background on image calibration methods and overviews the FINIS calibration plan. A step by step process for each of the calibrations is given in Appendix C.

6.1 Introduction to Image Calibration

Inherent in any image are offsets due to read noise, dark current, and non-uniformities caused by vignetting, dust spots, and uneven pixel gain. To extract the highest signal to noise ratio (SNR) from a scene, these offsets and irregularities need to be calibrated from the data collected from the FINIS instrument. These calibrations are better understood with a background on what happens to each camera pixel during data acquisition.

As photons enter a camera pixel they are converted to electrons based on the quantum efficiency (QE) of the camera. The Tau SWIR cameras used on FINIS have a QE of 60%, meaning they convert about 60% of incoming photons to electrons. Each camera pixel has what is referred to as a "well size," or the number of electrons that a pixel can hold during each acquisition. The number of electrons collected during an acquisition represent the intensity of light entering the pixel, and is recorded by the camera using an analog to digital converter (ADC).

Every image taken with a camera has a read noise associated with it, created by the process of measuring and draining electrons between acquisitions. Electrons left in the pixel wells create a bias in the number of electrons recorded, increasing the SNR. Read noise can be calibrated by taking a "flat dark." A flat dark is a completely black image taken at the camera's fastest exposure setting to limit other noise from being recorded. The flat dark can be subtracted from regular images to eliminate the effects of read noise.

Another source of noise in an image is the dark current. Thermal energy from the imaging sensor is converted to electrons in each pixel well, adding to the overall bias in an acquisition. The dark current is dependant on the temperature of the sensor and the length of exposure. Like taking a flat dark, a dark frame can be taken by acquiring a completely black image, but at the same gain and exposure as the camera uses during regular acquisition. A dark frame will also include electrons contributed by the read noise. Subtracting a dark frame from an image will remove the effects of dark current and read noise. Dark frame calibration will also remove the effects of hot pixels. For best results, several dark frames can be taken and averaged together [23].

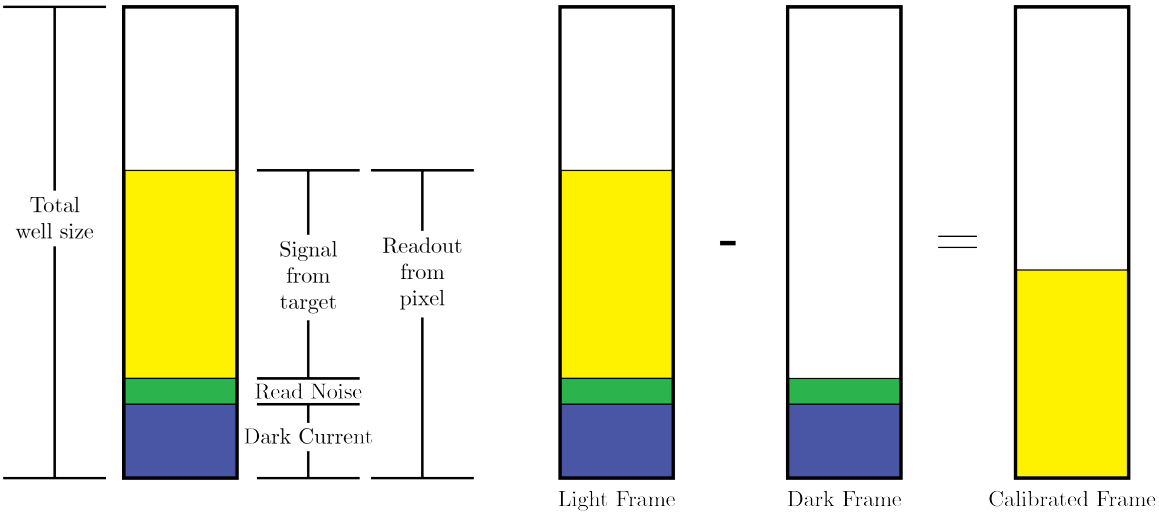

Fig. 6.1: Each pixel readout includes signal from the target, read noise, and dark current. The effects of read noise and dark current can be removed through calibration.

Also inherent in an image are non-uniformities from vignetting, dust spots, and uneven pixel gain. These effects can be calibrated through the use of flat frames. A flat frame is an image of a uniformly illuminated surface with an intensity that fills about half of the pixel well. Like other images, a flat image will have read noise and dark current incorporated in the measurement that need to be subtracted from each pixel. After the noise is subtracted, the gain is calibrated for each pixel to match a uniform field, thus removing the non-uniform effects. The gain of each pixel calculated for this transformation can then be used

to calibrate the gain pixels in subsequent images [24].

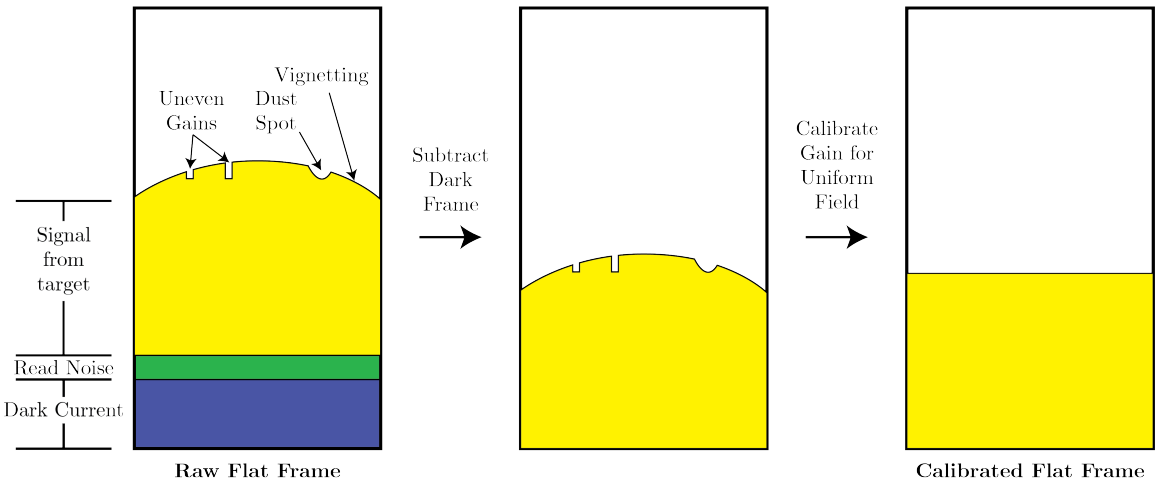

Fig. 6.2: Each image represents a line of pixels across the FPA. After subtracting the dark current, the gain of the pixels can be calibrated to match a uniform field.

Finally, a radiometric calibration is needed to convert digital units (number of electrons recorded by the ADC) to physical units. This can be done by either imaging a flat field of known radiance, or by taking flat frames with fields of two intensity levels and computing the slope between the outputs. A dark frame can be used as a third point to determine the offset. The correlation between intensity changes and number of electrons collected is linear, so the slope can be used to interpolate the intensity at any point.

6.2 Ground Calibration Plan

During lab testing, calibrations will be performed for the read noise, dark current, dark stability, system gain, and radiometric conversion of the cameras. Tests will also be run to characterize the point spread function (PSF), geometric corrections, and the spectrum across the FPA. Data can then be acquired with the instrument observing a known concentration of CH_4 and compared to the theoretical performance.

To ensure the darkest scene possible, the read noise and dark current tests will be performed in a completely dark room with the lens cover on the camera and the shutter closed. The

tests will be performed as described in section 6.1, with the addition of a dark stability test. The stability of the dark current will be measured by setting the camera TEC to 0° C and taking a dark frame every minute for 60 minutes.

Flat frames will be collected using the infrared calibration source discussed in section 4.5 and following the method discussed in section 6.1. The radiometric test will be performed by imaging the flat field with the LEDs set to a different intensity for each image. The slope between the data points is used to create a linear equation for the digital number to intensity conversion.

The PSF is a measure of how the light entering a single pixel impacts the pixels around it. This can be measured by imaging a light source that fills exactly one pixel and looking at the bleed to other pixels. Geometric corrections can be made by imaging a checkerboard pattern and correcting distortions in the image. The spectrum across the FPA is characterized by imaging specific wavelengths created by a monochromator.

Once the calibrations are performed, the instrument performance can be measured by imaging a known concentration of CH_4 in a test cell and comparing the image to a vacuum test cell. The length and pressure of the cell are changed to create varying concentrations of CH_4, and then the analyzed data is compared to the theoretical concentrations.

6.3 On-Orbit Calibration Plan

The FINIS instrument is designed to perform read noise, dark current, dark current stability, system gain, and radiometric calibrations on orbit. Calibrations are performed before each data acquisition, and are performed in the same manner as during lab testing.

CHAPTER 7

OPERATING MODES

This chapter outlines the operating modes for the FINIS instrument.

7.1 Off

When the spacecraft enters a low power or safety mode, all electronics for the FINIS instrument will be turned off.

7.2 Standby

When in standby, the camera TEC's will be active to maintain a sensor temperature of 0° C. The system is in standby between data acquisitions.

7.3 Calibration

Calibrations are run before each data acquisition. When in calibration mode, the solenoid is activated to hold the shutter in the closed position and the TEC maintains temperature at 0° C. With the shutter closed, the cameras then acquire dark frames. After dark frames are collected the infrared LEDs are turned on and flat frames are acquired. When the calibration process has ended the shutter returns to the open position and the LEDs are turned off.

7.4 Acquisition

The system enters acquisition mode when over land, in daylight, and with SZA $< 45°$. During acquisition the TEC maintains the sensor temperature at 0° C and images are acquired at a set rate and exposure.

CHAPTER 8

DATA ANALYSIS

Data analysis will be performed on the ground after science data is received from the spacecraft. USU PhD student Bruno Mattos is developing a CH_4 retrieval algorithm to process the science data. Two processing techniques are being investigated for optimum CH_4 concentration retrieval, the first is Differential Optical Absorption Spectroscopy (DOAS) and the second is an image ratio technique. Both methods will be implemented and then validated against a network of known CH_4 concentrations across the earth. A detailed analysis of the data processing methods will be written in Bruno's dissertation, so only a brief explanation is given here.

8.1 DOAS

DOAS is a method used to derive the concentrations of trace gases imaged with a multi-spectral sensor. The algorithm requires the gases of interest to be observed in two spectra, one where the gas is absorbed and one where the gas is largely transmitted. The cross sections and spectra of the gases known to be in the image are ran through a least squares estimation along with the geometry of the light paths to estimate the concentration of each gas type. Using DOAS on the FINIS data will allow for approximating the contribution of CH_4, H_2O, aerosols, and albedo on measurement data [25].

8.2 Image Ratio

The image ratio technique is a naive approach to retrieving CH_4 concentration in that it doesn't take the contributions of other gasses into consideration. This is the method used on the original FINIS system. After calibrations are performed on the images, the ground locations are matched pixel for pixel and a ratio is taken of the ground location

observed in the absorption and transmission bands. The ratio is interpolated to output CH_4 concentration.

8.3 Expected Performance

Based on the current output from Bruno's model, the FINIS instrument one-sigma sensitivity is approximately 3% of the CH_4 background, or roughly 54 ppb. Factors that affect this are exposure time, number of frames collected, temperature of the atmosphere, and albedo. While the sensitivity is lower than some of the leading CH_4 instruments today, it is sufficient to detect and measure leak rates of 500 kg/hr. According to the EPA Greenhouse Gas Reporting Program, 60% of US point source CH_4 emissions come from emitters with leak rates greater than 500 kg/hr [26].

8.4 Validation Method

The FINIS measurements will be validated using CH_4 measurements from the Total Carbon Column Network (TCCON) hosted by CalTech [27].

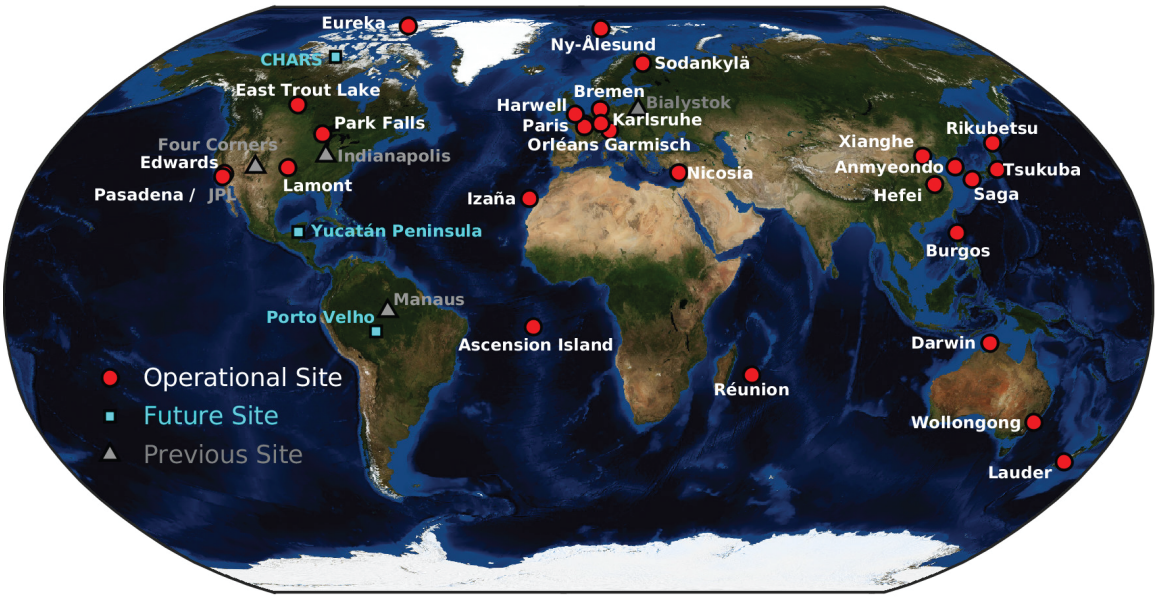

Fig. 8.1: Map of TCCON measurement locations [27]

CHAPTER 9

CONCLUSION

During the course of this thesis project, the FINIS instrument has been adapted and prepared for manufacturing, testing, and implementation on the ACMES mission. The final instrument design caters to a CubeSat form factor with a low size, weight, and power. The current theoretical model for the instrument performance indicates it will be comparable to other remote CH_4 sensors and will thus aid in reducing global greenhouse gasses. Many of the selected components have flight heritage and analysis has been done to show they will survive during the lifetime of the mission.

The FINIS instrument has the potential to make an immediate impact on global warming by identifying point source leaks of CH_4. Identification of leak sources will enable us to reduce anthropogenic emissions from fossil fuels, waste, and agricultural sources. FINIS' low size, weight, and power make it more cost effective than other remote CH_4 instruments, making it possible to employ multiple satellites and repeat ground overpasses more frequently.

FINIS uses the science of absorption spectroscopy to retrieve CH_4 concentrations in the atmosphere. The novel idea that makes FINIS instrument possible is the use of a tilted interference filter to create a spectrum around the 1666 nm CH_4 absorption feature. The 10° tilt of the filter makes it possible to view a spectrum of 10 nm around the peak absorption feature to include both CH_4 and H_2O absorption lines.

Since the conception of the project, the FINIS instrument has undergone several design iterations to bring it to an optimized state for CubeSat integration. The original design implemented a folded optical path with a single camera, but has been updated to a straight optical path with two imaging detectors. Each design iteration brought the instrument closer to its final, optimized state.

Part of the genius behind the FINIS instrument is the simplicity of its design. The system includes two cameras, optical components inside of lens tubes, and a shutter mechanism for onboard calibration. Most of the components are COTS parts with high TRL, thus reducing cost, complexity, and risk. The materials have also been analyzed for outgassing characteristics, and the design incorporates methods to hold moving components in place during launch.

FINIS interfaces with the spacecraft using four threaded holes on the bottom of the optical plate. The instrument occupies a volume of 140x89x66 mm^3 (approximately 0.82U) and weighs 804 g. The electrical interface includes two camera breakout boards and a 10 pin connector that interface with an external FPGA. On average, FINIS consumes 5 W of power.

The calibration plan includes characterizing the read noise, dark current, dark current stability, system gain, radiometric calibration, geometric corrections, point spread function, and spectral characterization of the Tau SWIR cameras. Each calibration will be performed on the ground during lab testing, and then the read noise, dark current, dark current stability, system gain, and radiometric calibrations will be performed before acquisitions on orbit.

While in orbit, FINIS will have four operating modes: off, standby, calibration, and acquisition. The system will turn off when the spacecraft enters a safety or lower power mode, but will normally operate in standby. When preparing for an acquisition the system will first enter calibration and then acquisition modes before returning to standby.

After data is acquired it will be sent to the ground for processing and analysis. An algorithm is currently being developed to implement DOAS and image ratio techniques for retrieving CH_4 concentrations and mapping them to physical ground locations. Currently, FINIS is estimated to have a sensitivity of 3% of the CH_4 background, allowing capability to map 60% of CH_4 emissions in the US. The data collected from FINIS will be validated by comparing measurements to data from the TCCON network.

While the original scope for this project included fabricating the instrument and performing ground testing, contract problems have delayed the acquisition of critical components and the instrument has not yet been built. Fabrication is currently expected to begin near the start of 2023 and testing will begin thereafter. While it has not been possible to vibe test the instrument, thought has been given to components that may move during launch. Loctite will be applied to optical components, a pin puller will hold the shutter, and electrical connections will all be securely fastened. Future work for this project includes altering the pin puller design to be accessible from the bottom of the spacecraft, analyzing radiation effects on the optics, and modifying the optics to allow a single camera solution with a larger aperture.

REFERENCES

[1] H. S. F. Laboratory, "Hyti - hyperspectral thermal imager." [Online]. Available: https://www.hsfl.hawaii.edu/missions/hyti/

[2] U. S. E. P. Agency, "Importance of methane," 2021. [Online]. Available: https://www.epa.gov/gmi/importance-methane

[3] U. N. E. Programme, Climate, and C. A. Coalition, "Global methane assessment: Benefits and costs of mitigating methane emissions," 2021. [Online]. Available: https://www.ccacoalition.org/en/resources/global-methane-assessment-summary-decision-makers

[4] E. Dlugokencky, "Trends in atmospheric methane," 2022. [Online]. Available: https://gml.noaa.gov/ccgg/trends_ch4/

[5] C. for Space Engineering, "Usu finis final report december 2019," 2019.

[6] U. of Washington, "Methane (ch_4)." [Online]. Available: http://vpl.astro.washington.edu/spectra/ch4.htm

[7] E. S. Agency, "Sciamachy overview." [Online]. Available: https://earth.esa.int/eogateway/instruments/sciamachy/description

[8] O. S. C. Analysis and R. Tool, "Instrument: Sciamachy-nadir," 2018. [Online]. Available: https://space.oscar.wmo.int/instruments/view/sciamachy_nadir

[9] E. S. Agency, "Instrumental payload." [Online]. Available: https://sentinels.copernicus.eu/web/sentinel/missions/sentinel-5p/instrumental-payload

[10] E. O. Portal, "Gosat-2 (greenhouse gases observing satellite-2)/ibuki-2." [Online]. Available: https://directory.eoportal.org/web/eoportal/satellite-missions/g/gosat-2

[11] ——, "Prisma (hyperspectral precursor and application mission." [Online]. Available: https://directory.eoportal.org/web/eoportal/satellite-missions/p/prisma-hyperspectral

[12] E. S. Agency, "About ghgsat." [Online]. Available: https://earth.esa.int/eogateway/missions/ghgsat

[13] O. S. C. Analysis and R. Tool, "Instrument: Tropomi," 2021. [Online]. Available: https://space.oscar.wmo.int/instruments/view/tropomi

[14] webbtelescope.org, "Spectroscopy 101." [Online]. Available: https://webbtelescope.org/contents/articles/spectroscopy-101--introduction

[15] AFCRL, "The hitran database." [Online]. Available: https://hitran.org/

[16] Alluxa, "What are thin-film optical filters?" [Online]. Available: https://www.alluxa.com/learning-center/what-are-thin-film-optical-filters/

[17] ——, "Ultra-narrow bandpass filters." [Online]. Available: https://www.alluxa.com/optical-filters/ultra-series-optical-filters-and-coatings/bandpass-filters/ultra-narrow-bandpass-filters/

[18] ——, "Angle of incidence (aoi) and polarization." [Online]. Available: https://www.alluxa.com/optical-filter-specs/angle-of-incidence-aoi-and-polarization/

[19] EBAD, "Nea model 1120-04 pin puller." [Online]. Available: https://www.ebad.com/wp-content/uploads/2020/06/EBAD-2020-NEA-Model-1120-Pin-Puller-RND4.pdf

[20] N. GSFC, "Outgassing data table." [Online]. Available: https://outgassing.nasa.gov/outgassing-data-table

[21] Lord Corporation. (2004) Aeroglaze z306 flat black absorptive polyurethane, low outgassing. [Online]. Available: https://www.spacematdb.com/spacemat/manudatasheets/Aeroglaze%20z306.pdf

[22] Harwin, "Outgassing in harwin products." [Online]. Available: https://www.harwin.com/support/articles/outgassing-in-harwin-products/

[23] J. Minnick, "Astrophotography, pixel by pixel: Part 6 - dirty buckets and calibration frames." [Online]. Available: https://cloudbreakoptics.com/blogs/news/astrophotography-pixel-by-pixel-part-6-things-you-dont-want-in-your-bucket-and-calibration-frames

[24] ——, "Astrophotography, pixel by pixel: Part 7 - how to get flat abs...i mean frames." [Online]. Available: https://cloudbreakoptics.com/blogs/news/astrophotography-pixel-by-pixel-part-7-flat-abs-i-mean-flat-frames

[25] C. McLinden, "Differential optical absorption spectroscopy." [Online]. Available: https://www.ess.uci.edu/~cmclinden/link/xx/node67.html

[26] EPA, "Greenhouse gas reporting program (ghgrp)." [Online]. Available: https://www.epa.gov/ghgreporting

[27] CalTech, "Total carbon column observing network (tccon)." [Online]. Available: https://tccondata.org/

APPENDICES

APPENDIX A

DESIGN ITERATIONS

This appendix includes images of the FINIS design iterations.

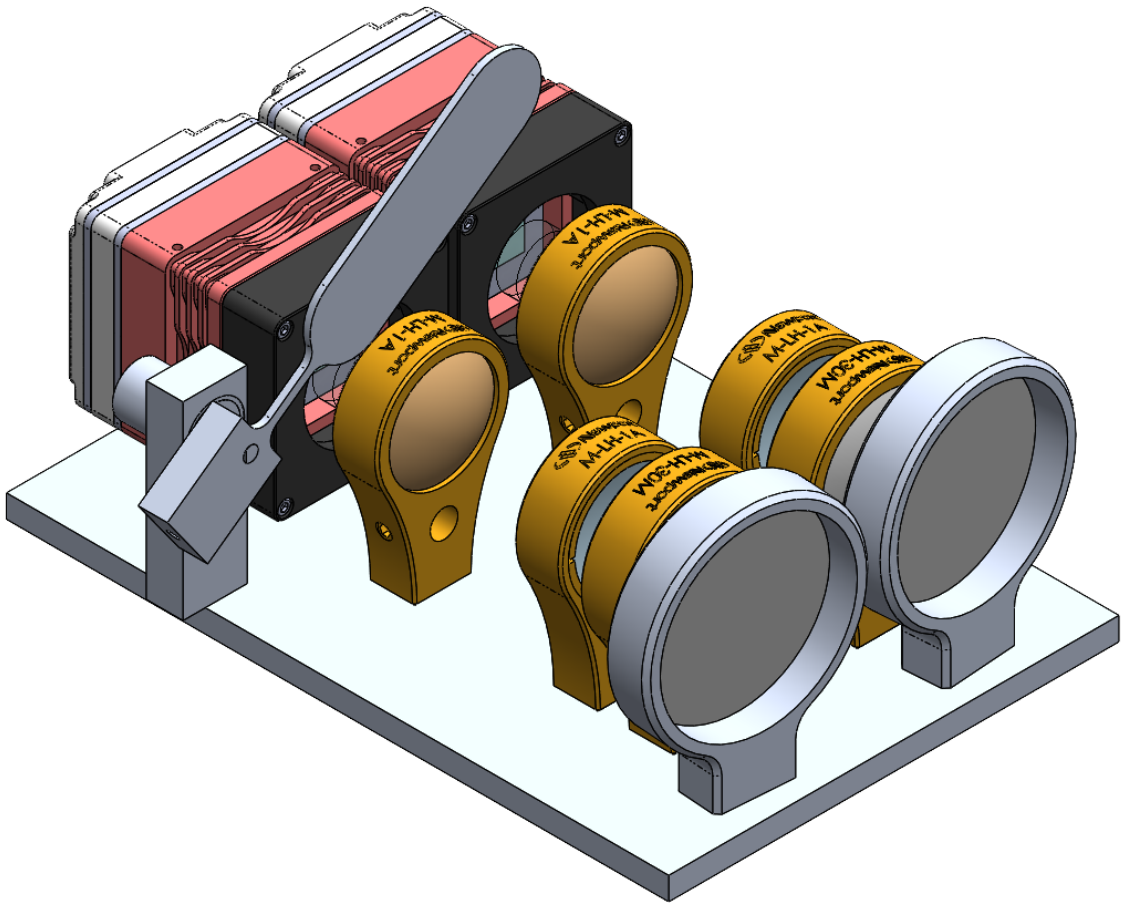

Fig. A.1: Rev 1 and 2 - The Goldeye camera is replaced with the Flir Tau SWIR and the fold mirror is removed in favor of a straight optical path. The optical components are mounted with the same style of mounts as the original FINIS design. The shutter arm is elongated to cover the apertures of both cameras.

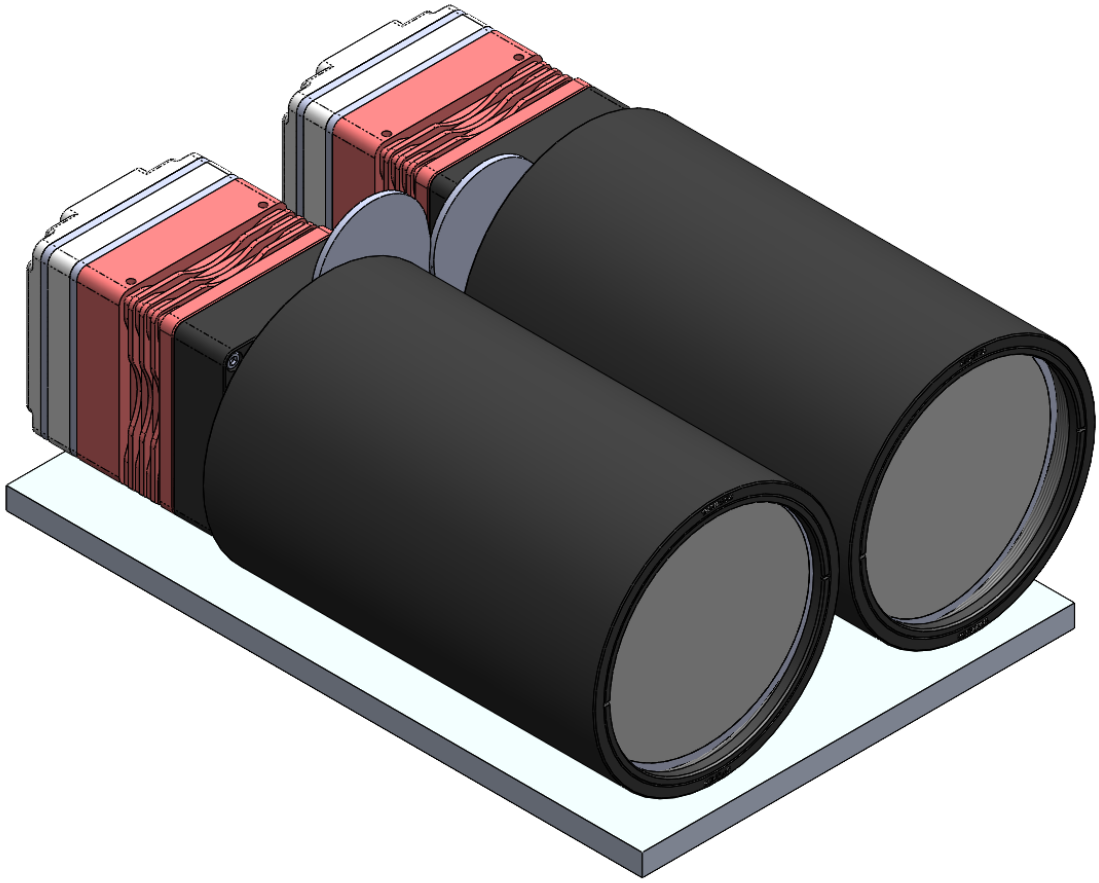

Fig. A.2: Rev 3 - A lens tube approach is used to mount the optical components. At this point in the design, a single COTS lens tube holds all the lenses, with the idea that adapter mounts will be built for each lens to screw into the main tube. A larger aperture was implemented to give a higher signal to noise ratio. During this revision several shutter designs were investigated. The final shutter design during this revision is a single mount in between the cameras with two solenoid actuators.

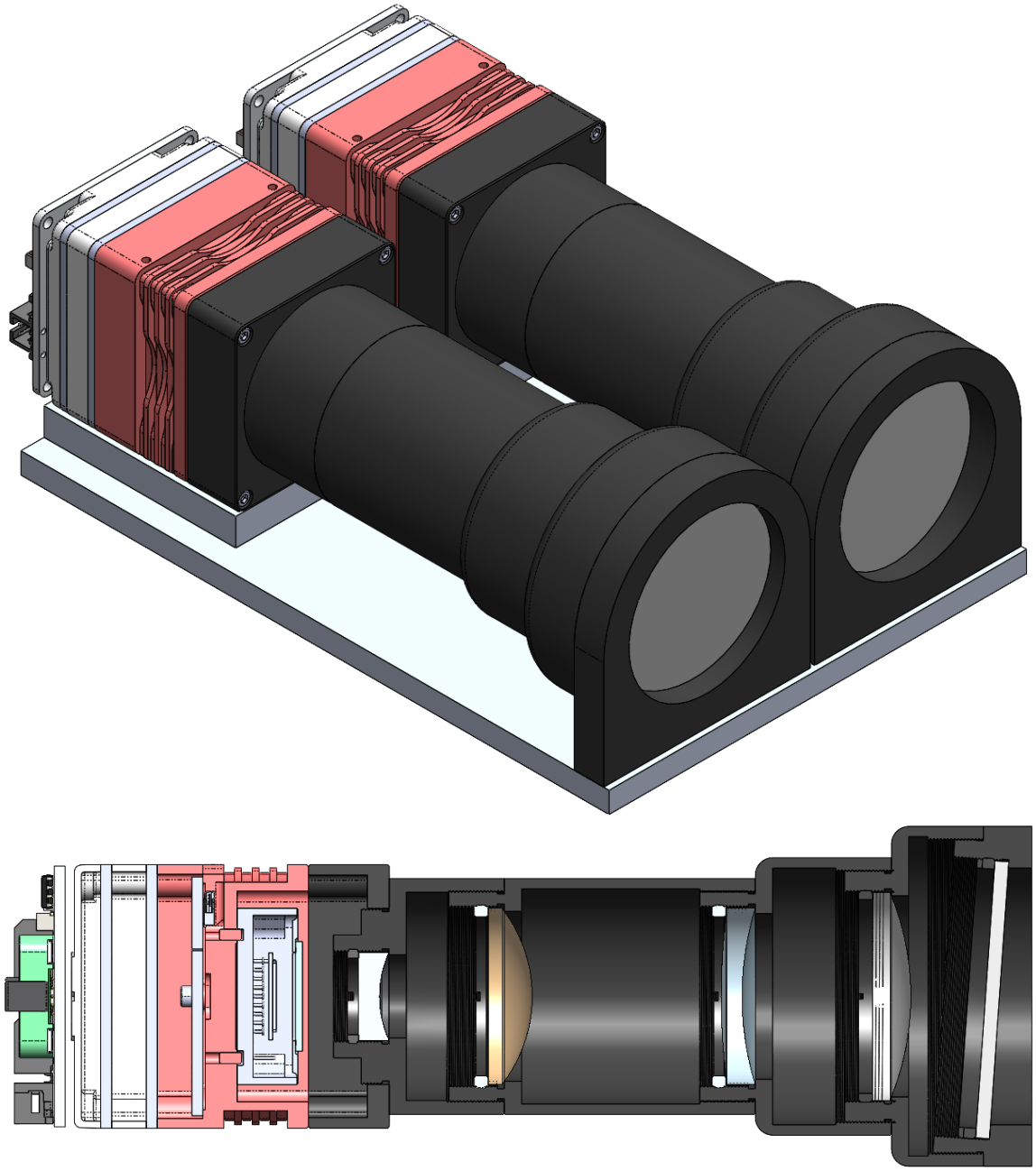

Fig. A.3: Rev 4 - The lens tube is refined to minimize size and mass. Each lens is held by a custom piece of the lens tube and the front piece mounts to the optical bench. The interference filter is changed back to 40mm as changing optics for a larger aperture is not reasonable. The shutter is removed from the design due to concerns from OSS about risks from adding a moving mechanism.

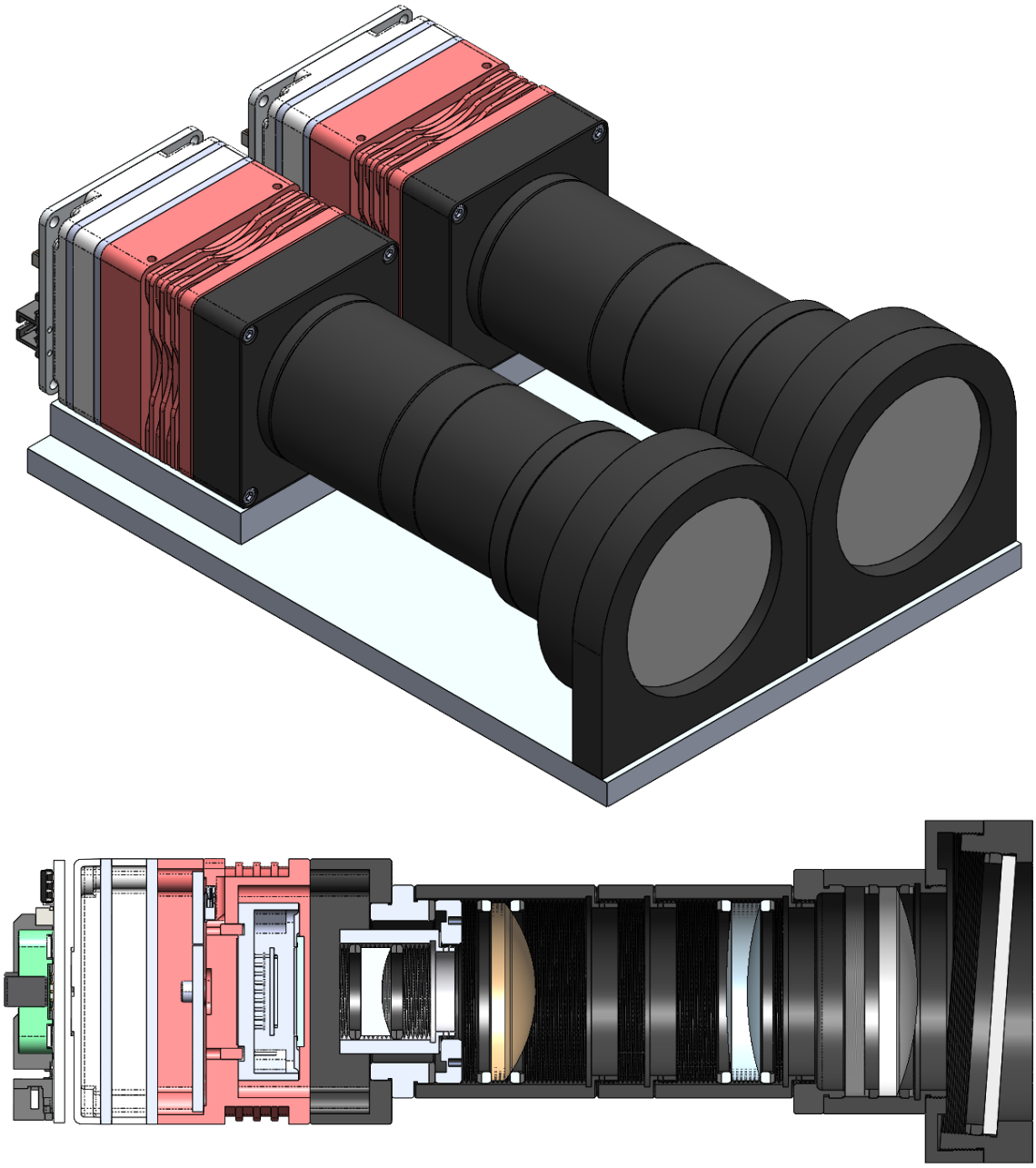

Fig. A.4: Rev 5 - The custom lens tube pieces are replaced with COTS lens tubes to reduce instrument costs. The only custom piece is the mount for the interference filter.

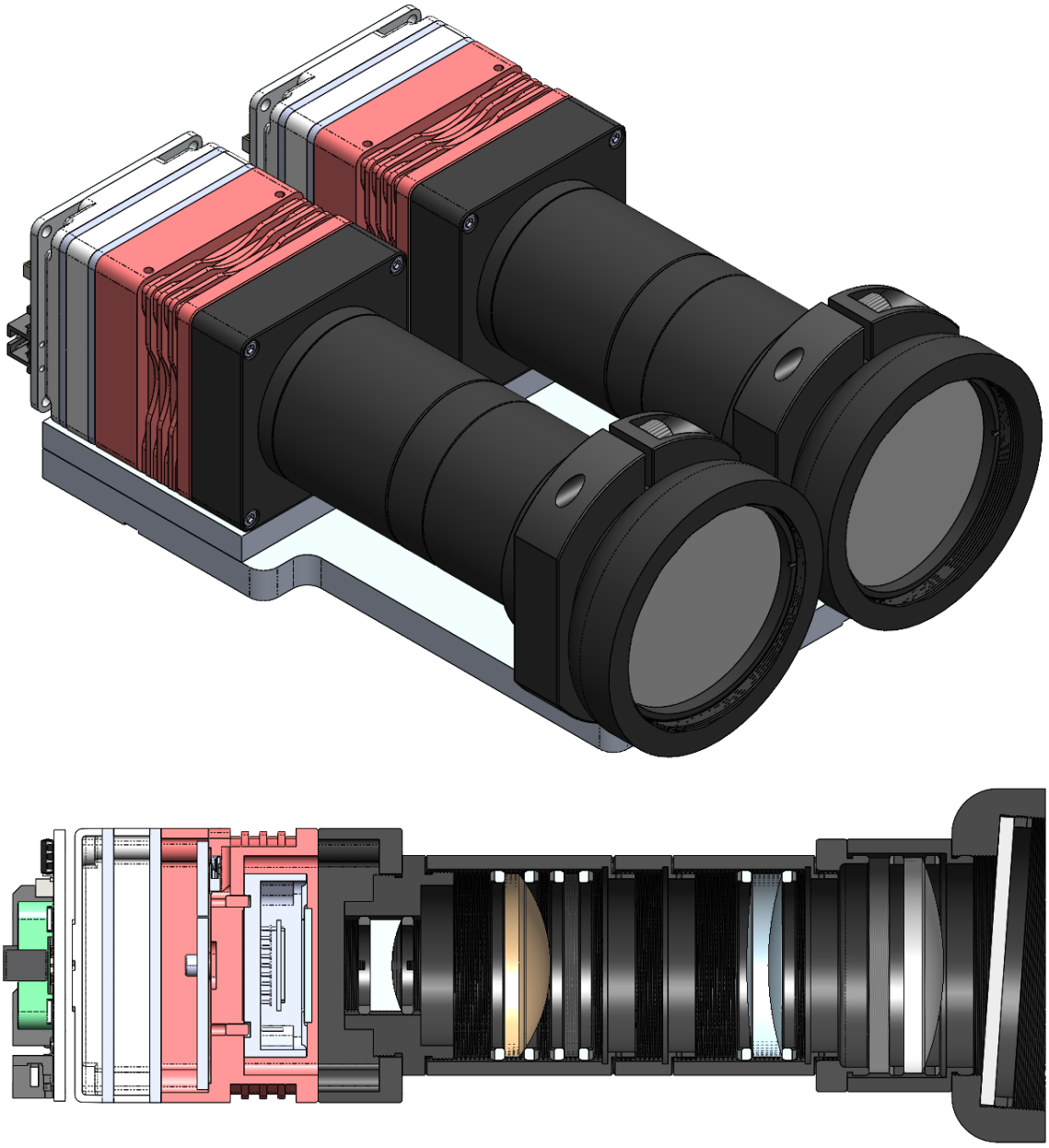

Fig. A.5: Rev 6 - The L4 Mount is switched from COTS components to a custom piece because the COTS components obstructed the optical path. The interference filter mount is also changed to reduce the number of lens tube components and simplify the mounting method.

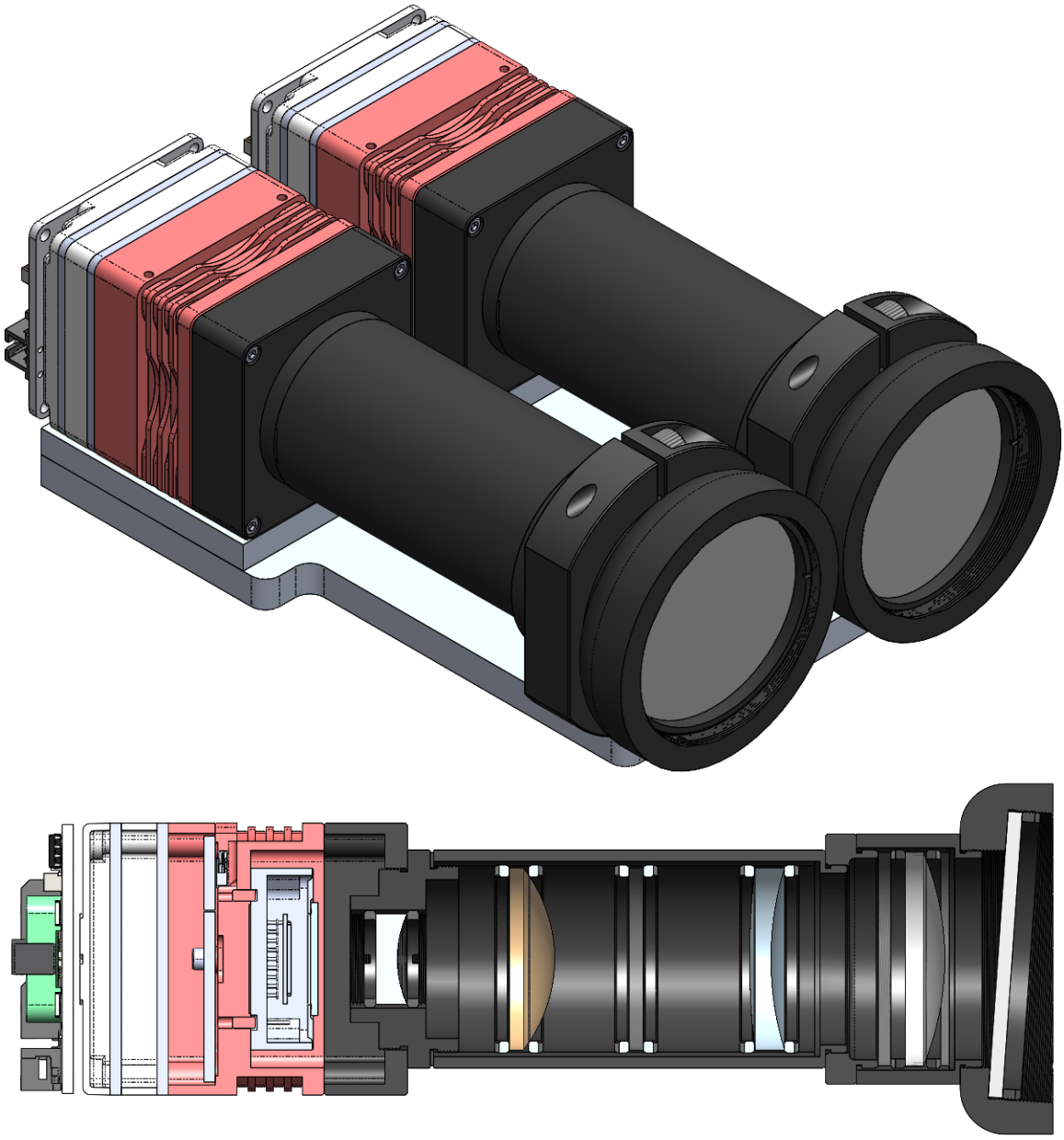

Fig. A.6: Rev 7 - The lens tube components are simplified further to reduce the number of pieces.

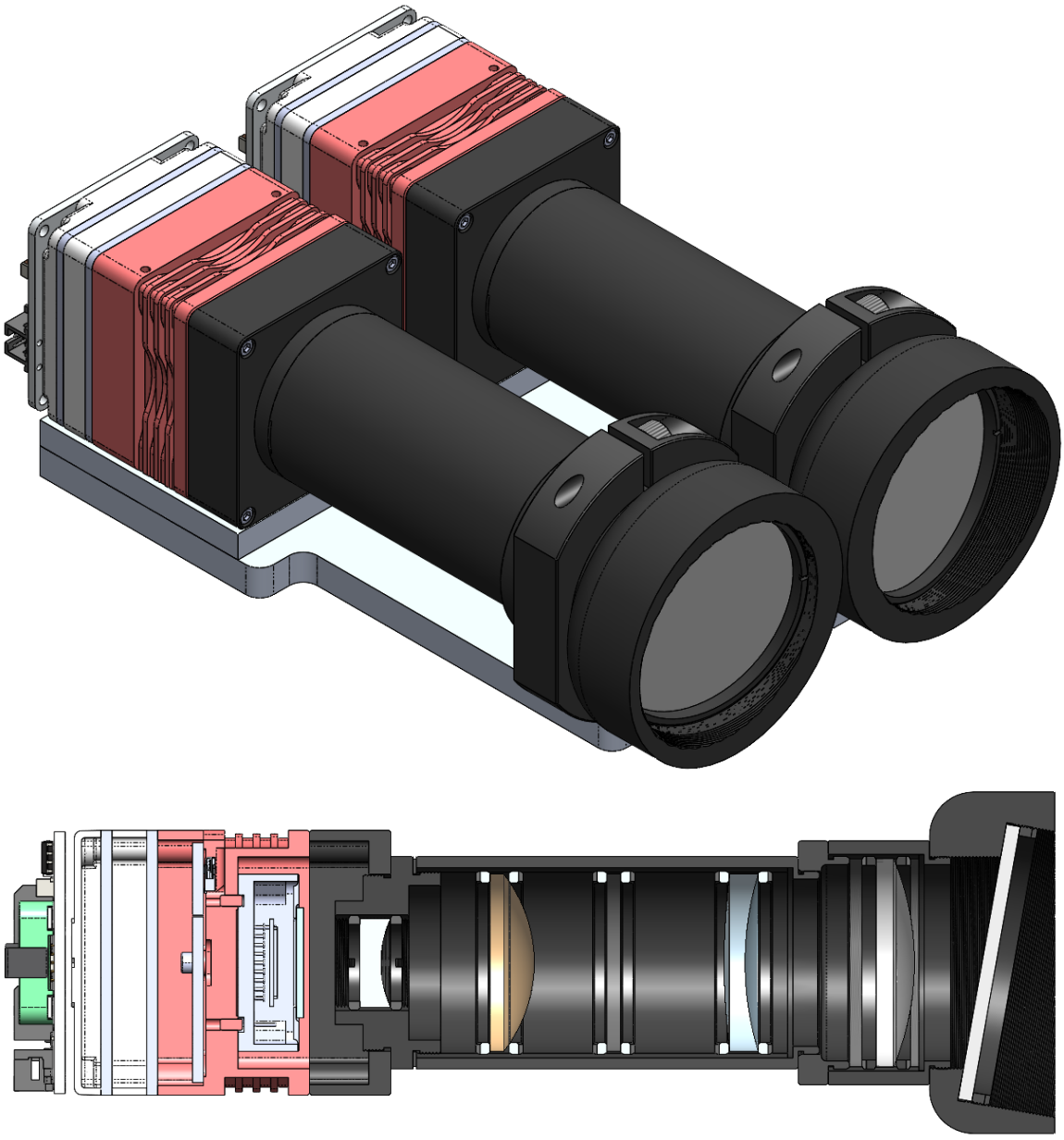

Fig. A.7: Rev 8 - The tilt of the interference filter is changed from 4 degrees to 10 degrees to provide a wider spectrum.

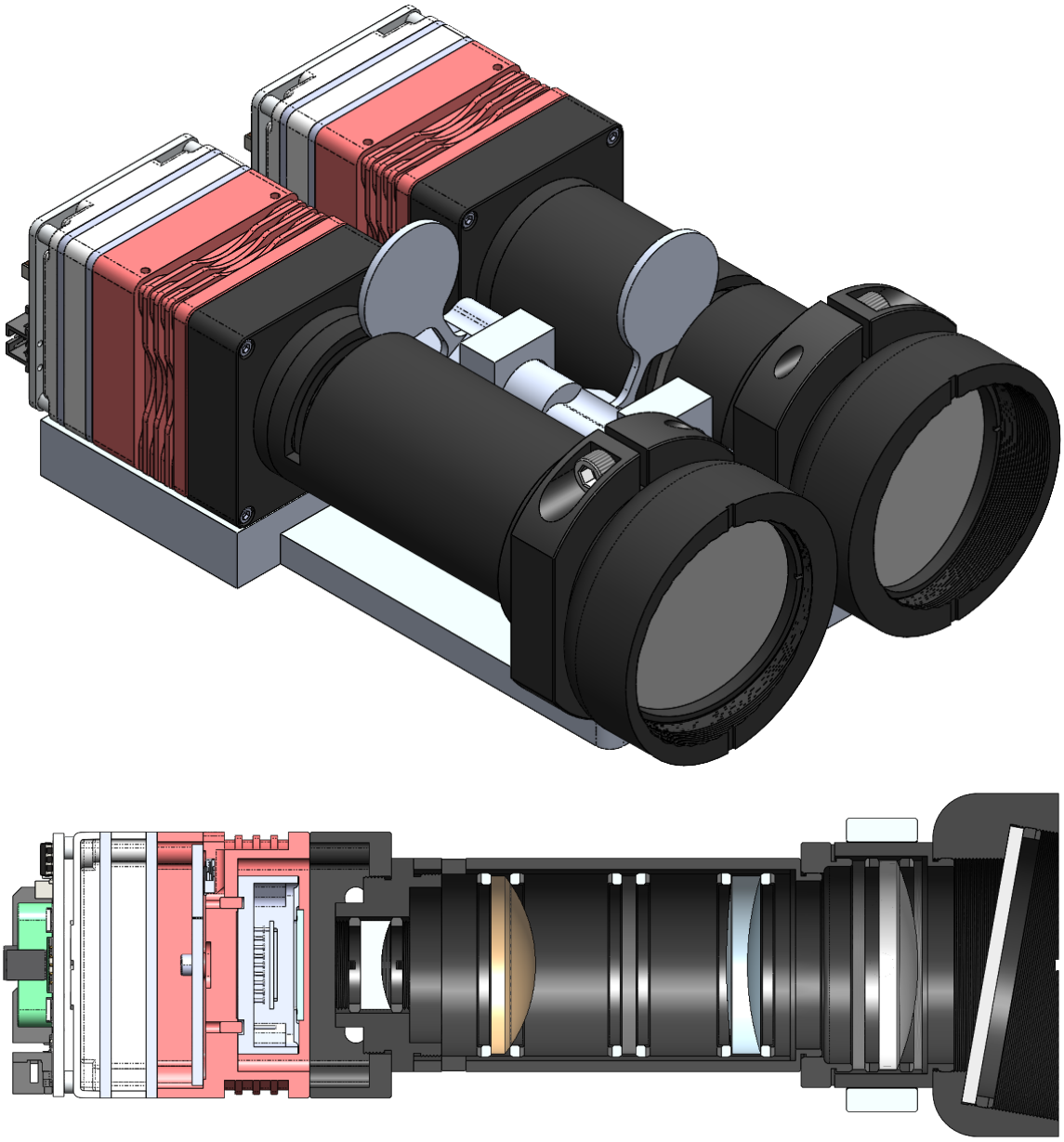

Fig. A.8: Rev 9 - Discussions with members of The Aerospace Corporation who have flown the Tau SWIR camera reveal that random hot pixels were common on the instrument sensor. As a result of the conversations, a shutter is added back to the instrument design to allow for onboard calibrations. The shutter is split into two mechanisms on either side of the instrument.

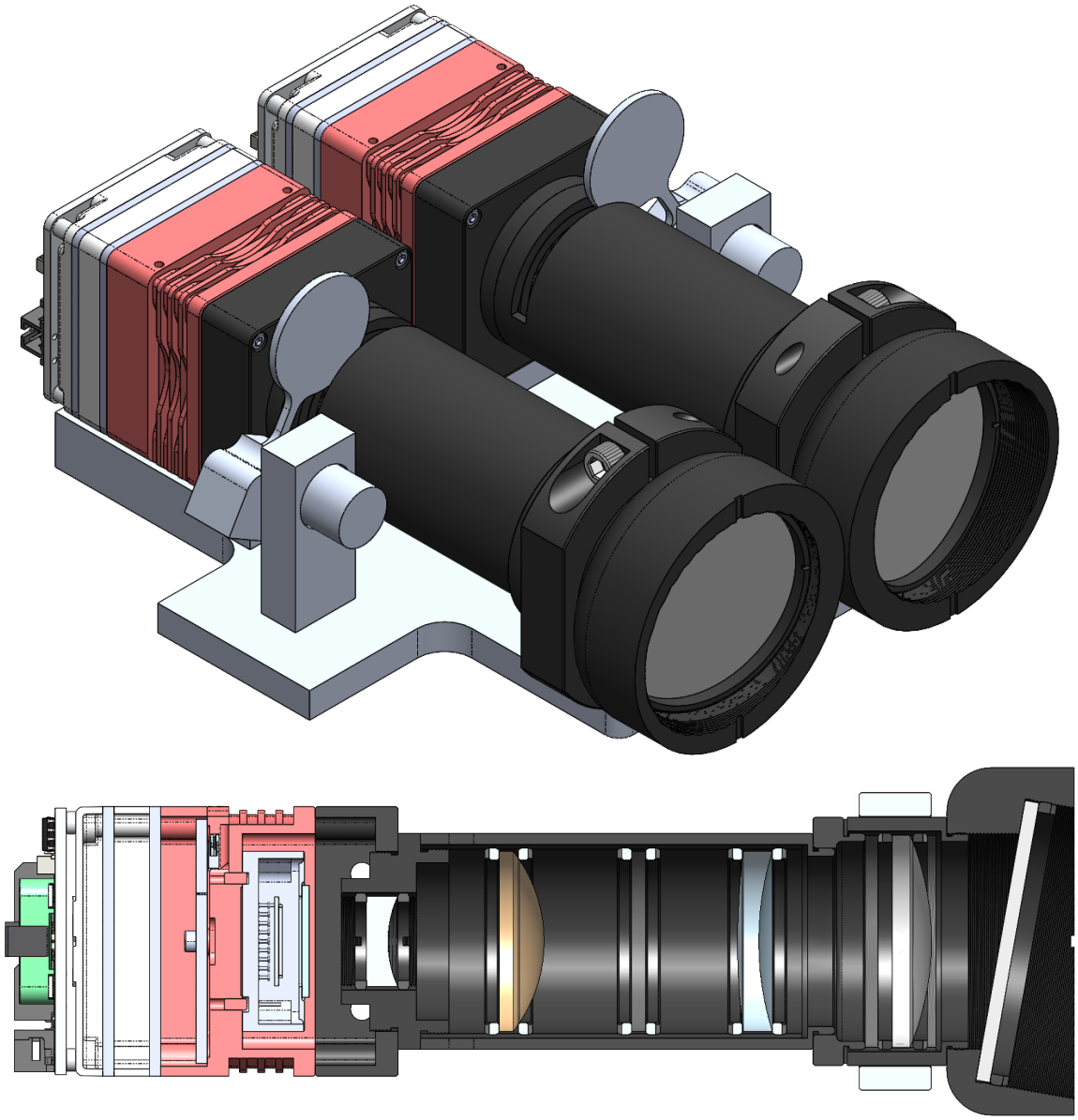

Fig. A.9: Rev 10 - The shutters are moved in between the lens tubes but offset from each other.

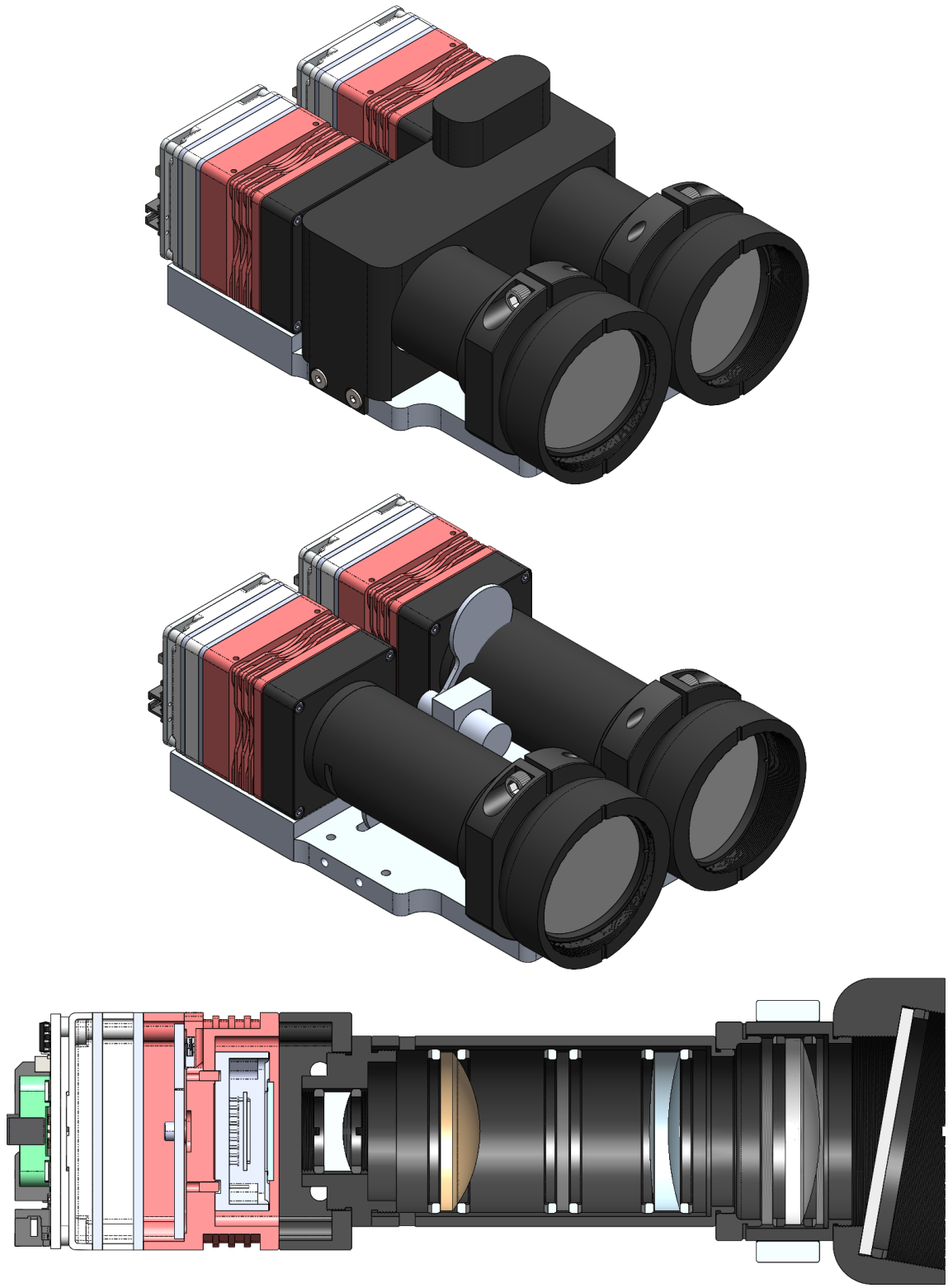

Fig. A.10: Rev 11 - The shutters are combined into a single shutter plane. A slot is cut into the optical bench to accommodate when the shutter is in the "open" position. A baffle is also implemented to prevent stray light from entering the lens tubes.

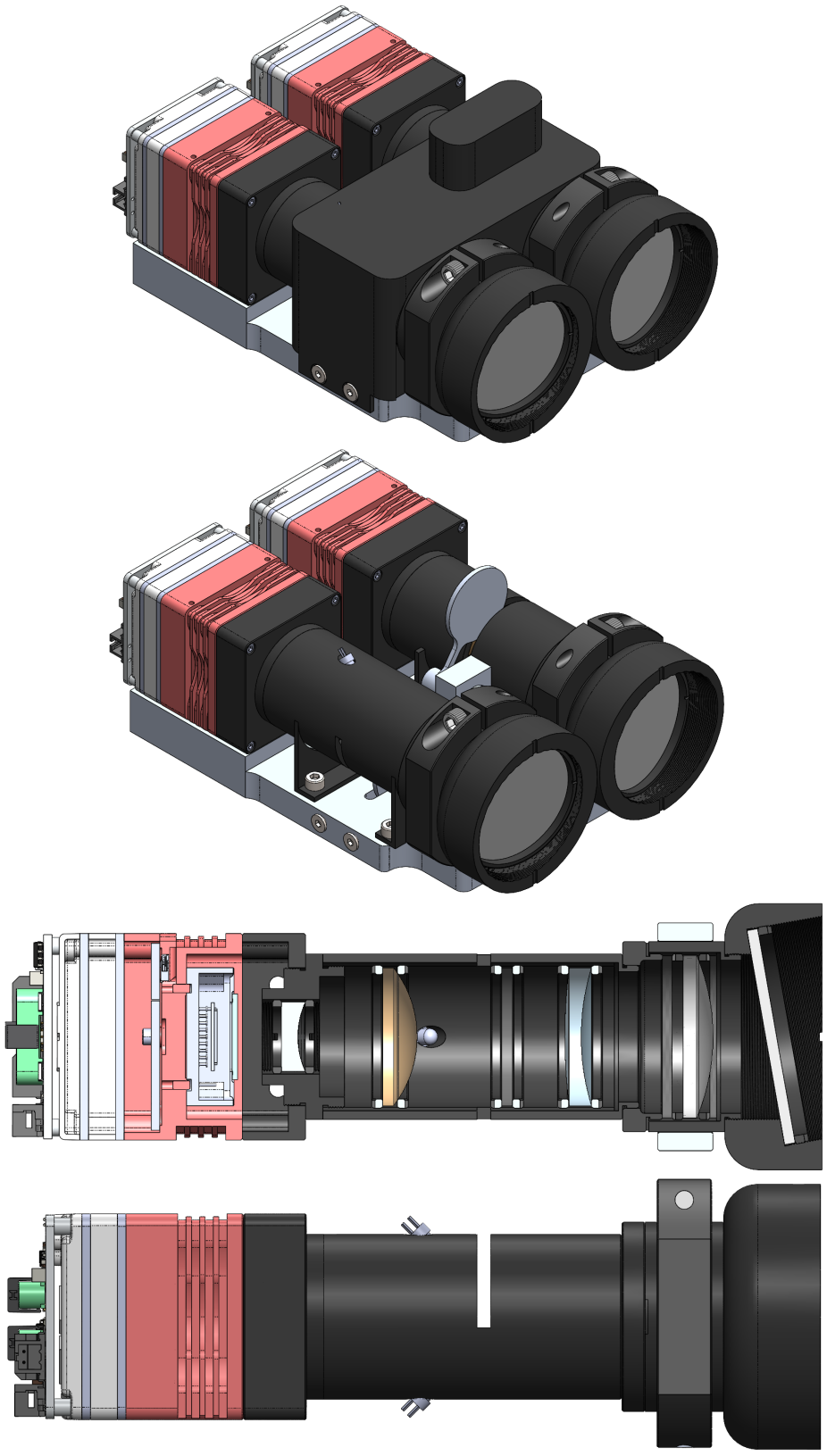

Fig. A.11: Rev 12 - Holes are added to the lens tubes to radially mount infrared LED's. The LED's will act as a calibration source while in orbit. As a result, the shutter is moved further along the optical path.

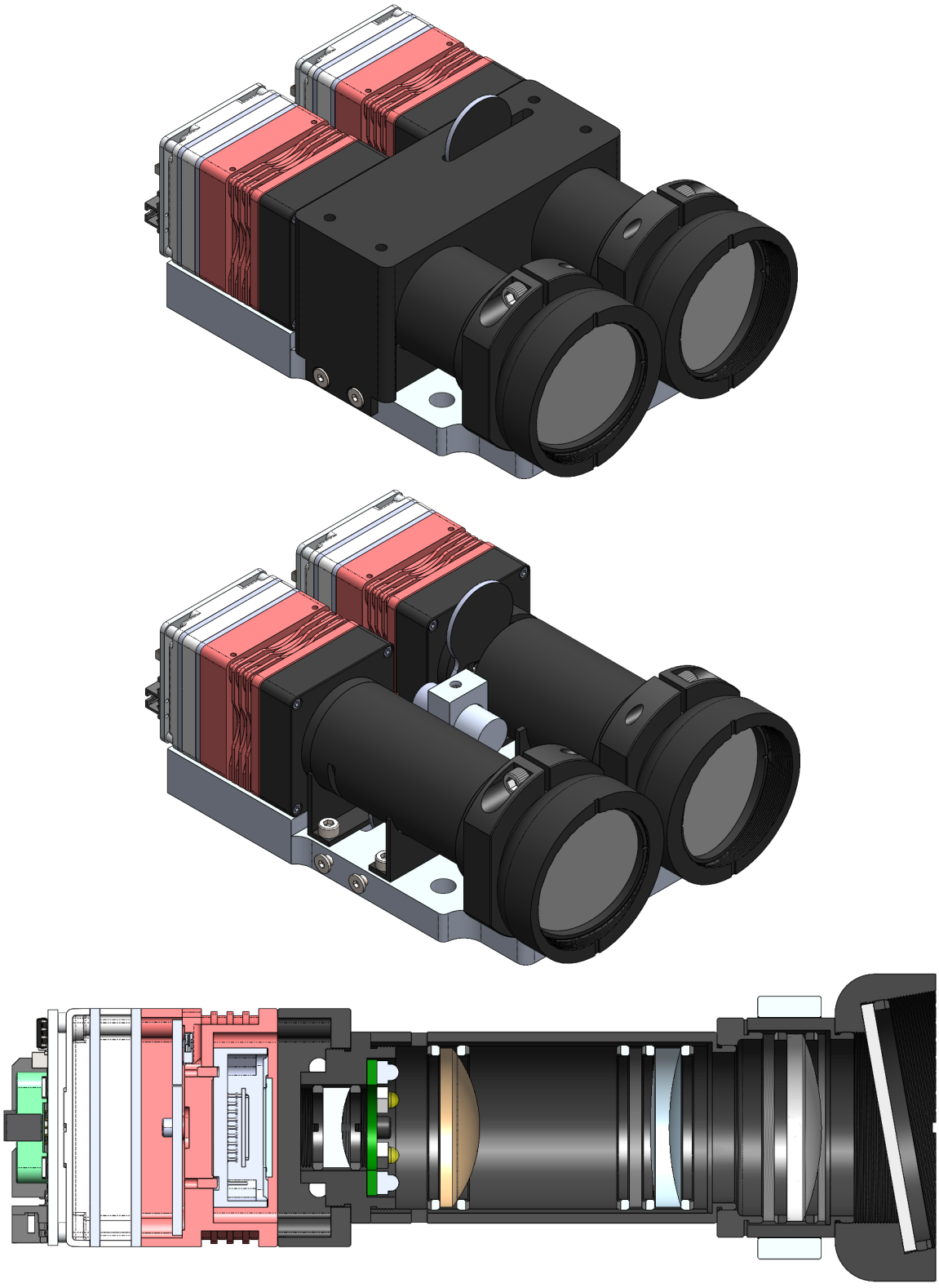

Fig. A.12: Rev 13 - The calibration source is changed from radially mounted LED's on the lens tube to LED's mounted on a circuit board inside the lens tubes. The shutter is moved back to its location after L3, and the shutter protrusion on the baffle is removed to allow the FPGA board to be mounted on top of the baffle.

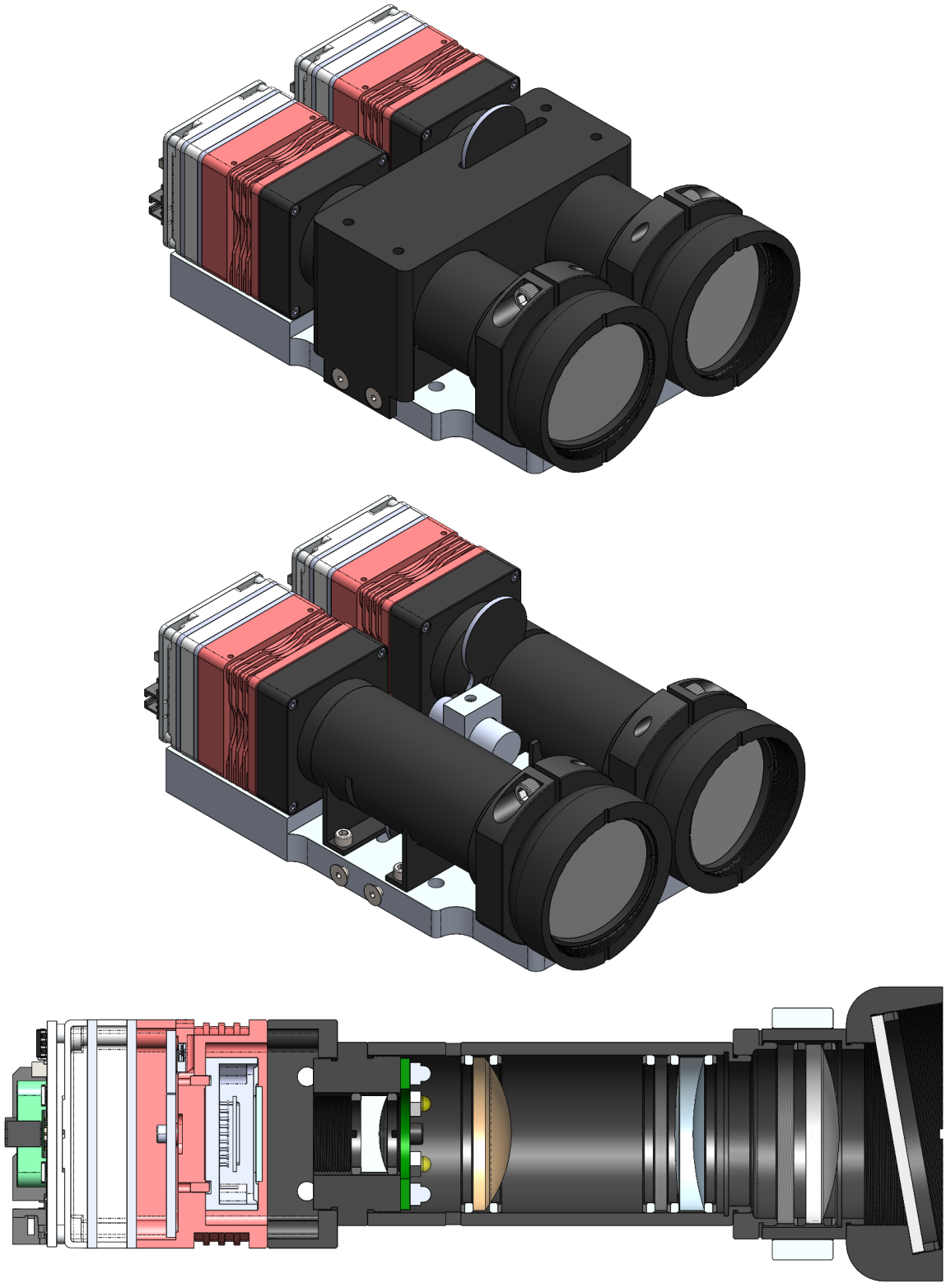

Fig. A.13: Rev 14 - Analysis from John Noto reveals that the optical focus of the instrument is incorrect. An attempt is made to fix it by increasing the distance between L4 and the instrument sensor.

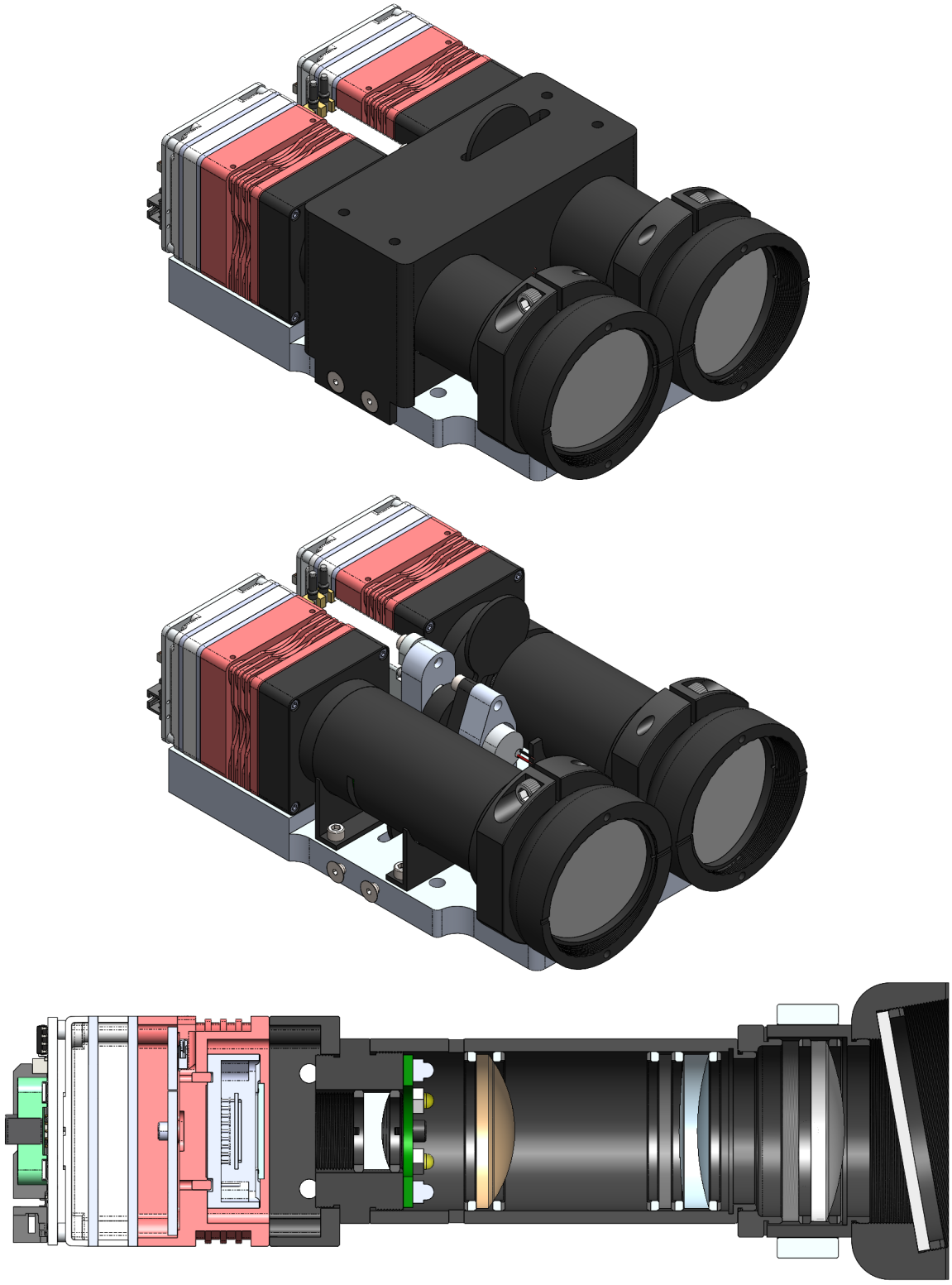

Fig. A.14: Rev 15 - Information from Brandstrom Instruments reveals that the solenoid is not strong enough to hold the shutter in place during launch vibrations. A pin puller from EBAD is implemented to hold the shutter.

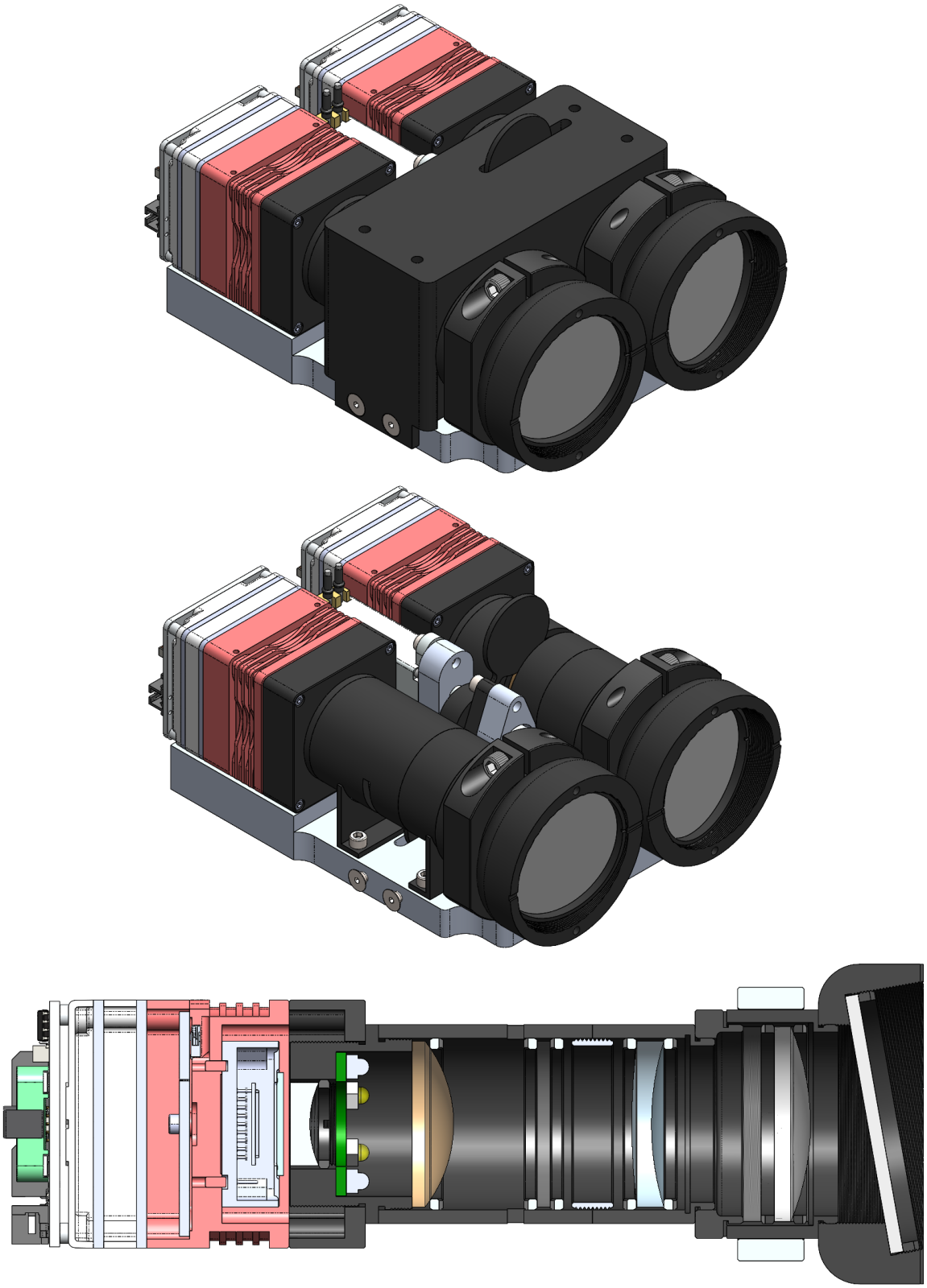

Fig. A.15: Rev 16 - More optical analysis from John Noto reveals the correct distance between L4 and the instrument sensor. The optics are moved closer to the detector and the lens tube components are adjusted to accommodate the changes.

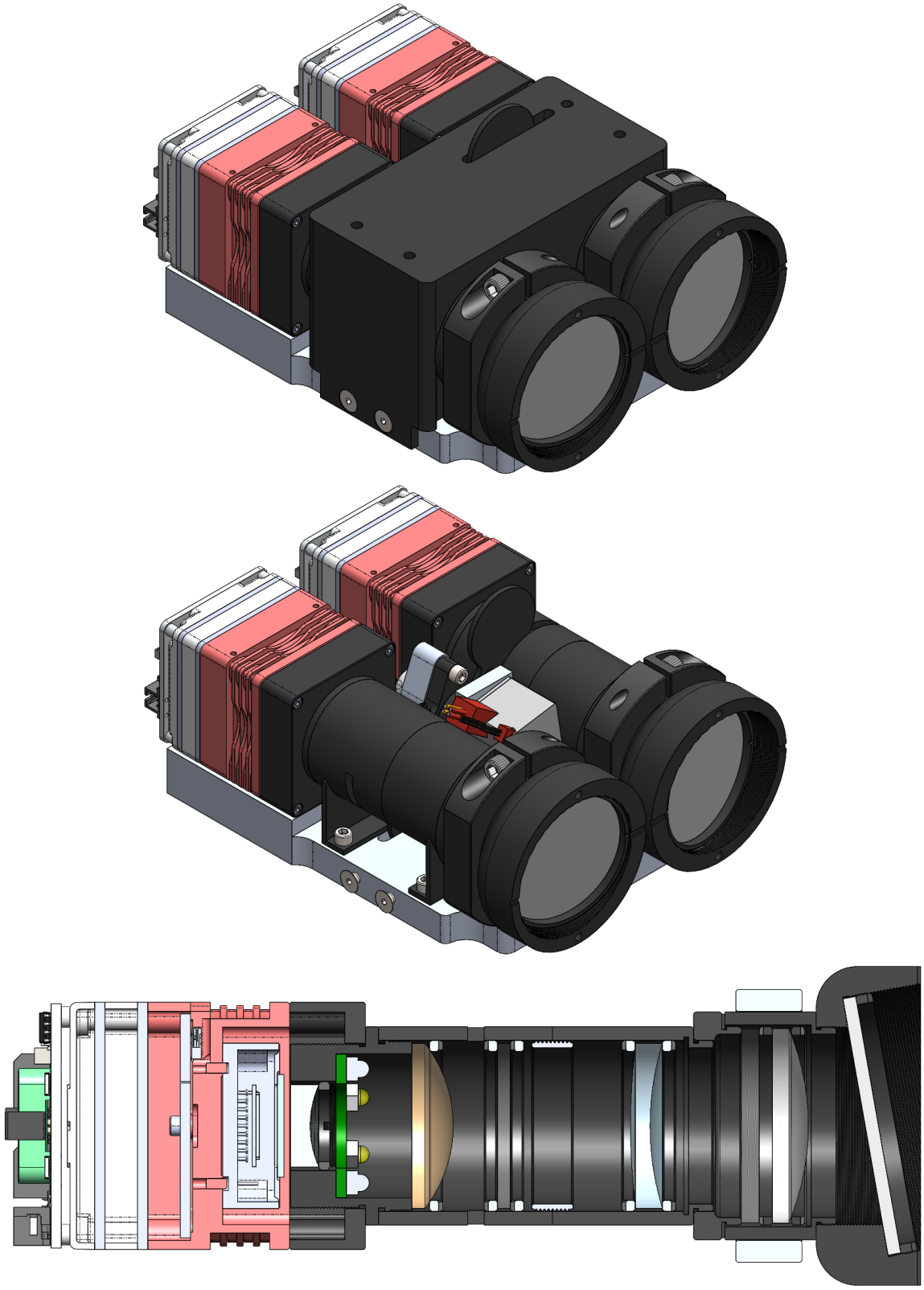

Fig. A.16: Rev 17 - The EBAD pin puller is switched to a nano pin puller from DCubed. The new pin puller is situated between the lens tubes instead of between the cameras and is fully resettable after actuation.

APPENDIX B

SCHEMATIC

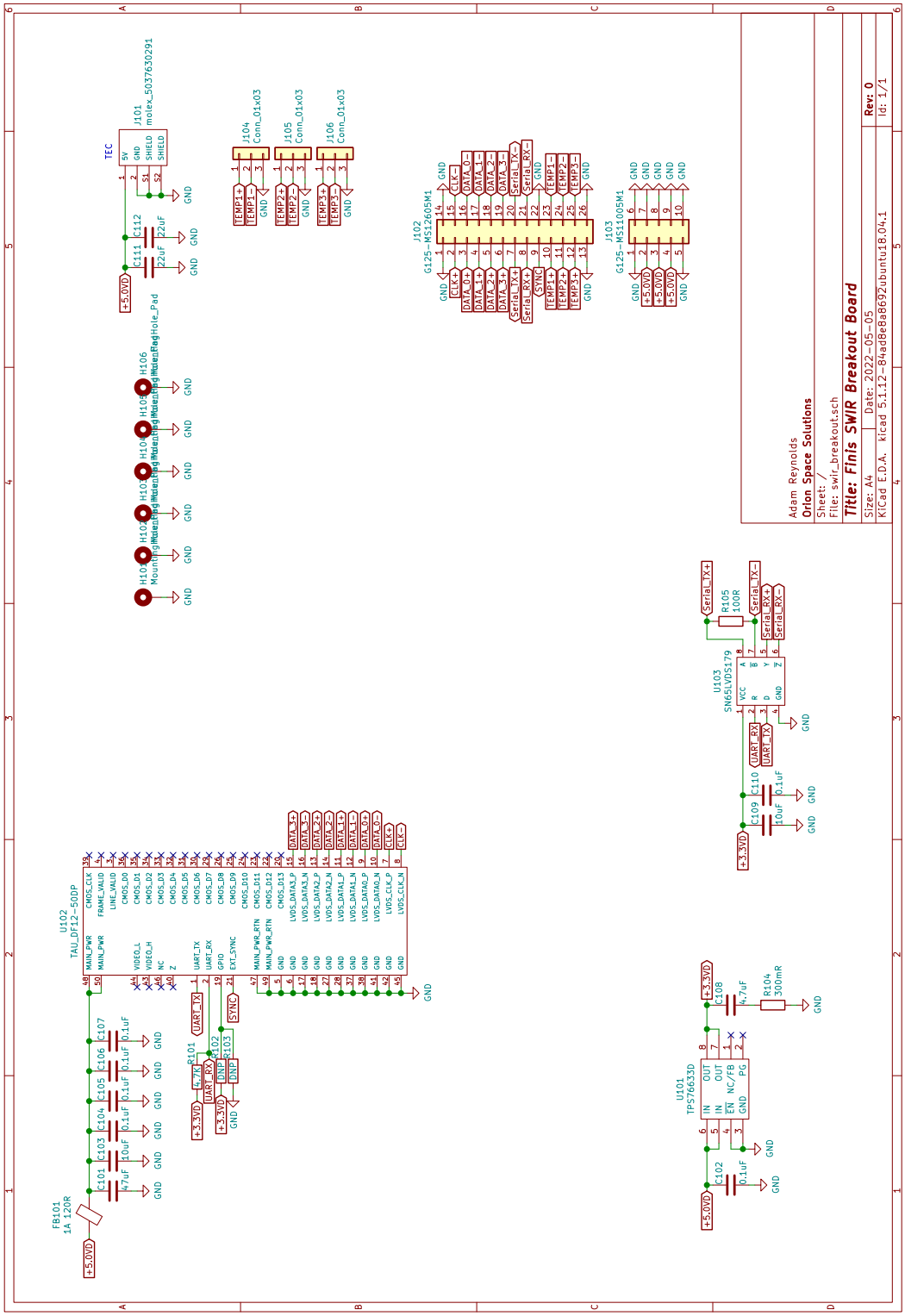

Fig. B.1: SWIR breakout board schematic

APPENDIX C

CALIBRATION STEPS

C.1 Read Noise

1. Create a completely dark environment for the FINIS System
2. Close the shutter and put the lens cover on the lens tube
3. Set the TEC to temperature stabilize the sensor at 0° C
4. Set the exposure of the cameras to the fastest setting
5. Take an image with both cameras
6. Record the reading from both images

C.2 Dark Current

1. Create a completely dark environment for the FINIS System
2. Close the shutter and put the lens cover on the lens tube
3. Set the TEC to temperature stabilize the sensor at 0° C
4. Set the exposure of the cameras to be the same as the exposure during data acquisition
5. Take an image with both cameras
6. Record the reading from both images
7. Subtract the read noise to obtain the total dark current count

C.3 Dark Current Stability

1. Create a completely dark environment for the FINIS System
2. Close the shutter and put the lens cover on the lens tube
3. Set the TEC to temperature stabilize the sensor at 0° C
4. Set the exposure of the cameras to be the same as the exposure during data acquisition
5. Take an image with both cameras every minute for one hour
6. Subtract the read noise from each image and plot the dark current over time to determine stability

C.4 System Gain

1. Create a completely dark environment for the FINIS System
2. Close the shutter and put the lens cover on the lens tube
3. Set the TEC to temperature stabilize the sensor at 0° C
4. Set the exposure of the cameras to be the same as the exposure during data acquisition
5. Turn on the infrared calibration source to set point 1
6. Take an image with both cameras
7. Subtract the dark frame from the images
8. Correct the gain pixel by pixel to create a uniform field across the FPA

C.5 Radiometric Calibration

1. Create a completely dark environment for the FINIS System
2. Close the shutter and put the lens cover on the lens tube
3. Set the TEC to temperature stabilize the sensor at 0° C

4. Set the exposure of the cameras to be the same as the exposure during data acquisition
5. Turn on the infrared calibration source to set point 1
6. Take an image with both cameras
7. Set the infrared calibration source to set point 2
8. Take an image with both cameras
9. Subtract the dark frame from the images
10. Find the slope of the intensity change for each pixel
11. Use the slope of the gain to convert digital units to physical units

C.6 Geometric Correction

1. Set up a checkerboard pattern perpendicular to the FINIS instrument in a way that it fills the entire image
2. Take an image with both cameras
3. Correct the images to match the checkerboard geometry

C.7 Point Spread Function

1. Determine a light source at a distance such that it fills exactly one pixel on the FPA
2. Take an image with both cameras
3. Quantify the light recorded by neighboring pixels

C.8 Spectral Characterization

1. Place a monochromator in front of the FINIS instrument
2. Set the monochromator to emit a wavelength at the low end of the FINIS instrument spectrum

3. Take an image with both cameras
4. Incrementally change the wavelength emitted from the monochromator and take images with each change in wavelength
5. Repeat until the whole FINIS spectrum has been imaged
6. Observe the radiation recorded in each image and correlate to the wavelength.

C.9 CH_4 Cell Testing

1. Pull vacuum on a test cell
2. Take an image of the test cell with both cameras
3. Fill the test cell with CH_4 to a given pressure
4. Take an image of the test cell with both cameras
5. Subtract the vacuum image from the CH_4 image to obtain the intensity of CH_4 values
6. Repeat the test with varying pressures and lengths of test cells to simulate varying concentrations.
7. Compare values to the theoretical performance of the instrument